J. Fluid Mech. (1978), *vol.* 87, *part* 2, *pp.* 349–383
Printed in Great Britain

The free shear layer tone phenomenon and probe interference

By A. K. M. F. HUSSAIN AND K. B. M. Q. ZAMAN
Department of Mechanical Engineering, University of Houston, Texas 77004

(Received 11 April 1977 and in revised form 7 November 1977)

Free shear layer stability measurements with a hot wire revealed that the probe itself can trigger and sustain upstream instability modes like the slit jet–wedge edge tones. The flow fields associated with the free shear layer tones induced in axisymmetric and plane air shear layers by a hot-wire probe and by a plane wedge were then explored experimentally, and found to be different in many ways from the widely investigated jet edge tone phenomenon.

As many as four frequency stages have been identified, there being a fifth stage associated with the subharmonic attributed to vortex pairing in the free shear layer. No evidence of hysteresis could be found in the shear layer tone. In the interstage jump (i.e. bimodal) regions, the tone occurred in only one mode at a time while intermittently switching from one to the other. Frequency variations in each stage are shown to collapse on a single curve when non-dimensionalized with the initial momentum thickness θ_e or with the lip–wedge distance h, and plotted as a function of h/θ_e.

Phase average measurements locked onto the tone fundamental show that the phase velocity and wavelength of the tone-induced velocity fluctuation are essentially independent of the stage of tone generation; in each stage, both phase velocity and wavelength decrease with increasing frequency but undergo jumps at starts of new stages. The measured amplitude and phase profiles, as well as the variations of the shear tone wavenumber and phase velocity with the Strouhal number, show reasonable agreement with the predictions of the spatial stability theory. The wavelength λ bears a unique relation to h, this h, λ relation being different from the Brown–Curle equation for the jet edge tone.

Shear layer tones would be typically induced in near-field shear layer measurements involving invasive probes, and can produce misleading results. A method for determining the true free shear layer natural instability frequency is recommended.

1. Motivation and introduction

1.1. *Introduction*

The developing region of free turbulent shear layers is dominated by large-scale quasi-deterministic structures which play the key role in entrainment and noise production (Browand & Laufer 1975; Brown & Roshko 1974; Bishop, Ffowcs Williams & Smith 1971; Liu 1974). Even in the self-preserving region where much of the turbulent kinetic energy has cascaded down – through nonlinear interactions – from these large scales to smaller scales, the large-scale coherent structure is believed to play the major role in the transport of momentum, heat and mass. Characteristics and roles

of organized structures and conditions favouring their formation and sustenance are of fundamental importance in turbulent shear flows (Liepmann 1976, private communication; Roshko 1976; Kovasznay 1977).

Some recent studies (Bradshaw 1966; Hussain & Clark 1977; Hussain & Zedan 1978*a*, *b*) show that the average measures of a free shear flow depend strongly on the initial condition, viz. the characteristics of the initial boundary layers producing these flows. (Thus it is likely that the large-scale organized structure in a turbulent free shear flow never achieves true self-preservation or local invariance in a finite flow length.) When the initial free shear layer is laminar, the wavelength of its most unstable mode, which depends on the velocity distribution, identifies the initial spacing of the rolled-up vortices and thus the initial large-scale size. However, these vortices may undergo interactions like coalescence (pairing or tearing) producing progressively larger scales of coherent motions (Brown & Roshko 1974; Winant & Browand 1974; Moore & Saffman 1975; Zaman & Hussain 1977). When the initial boundary layer is turbulent, its various integral measures like momentum thickness and shape factor, and turbulence characteristics like probability density and moments, Reynolds stress and spectra, may be taken as the identifiers of its initial condition. It is also possible that an initially turbulent free shear layer can roll up into organized large-scale vortical motions which then evolve not unlike the initially laminar case.

Very little is known about the effects of the initial condition on the development of free turbulent shear flows (Kline *et al.* 1973; Hussain 1977) or about the effect of controlled periodic excitation on the near-field large-scale coherent structure of free shear flow (Crow & Champagne 1971; Hussain & Thompson 1975; Hussain & Zaman 1977). This paper is an offshoot of our continuing investigation obtaining basic information in this area.

While flow visualization can be highly effective in understanding qualitatively the large-scale coherent structures and their kinematics, a hot wire is the commonly employed tool for acquiring quantitative and accurate aerodynamic data. During hot-wire measurements of the natural roll-up frequencies of initially laminar free shear layers, in connexion with our study of controlled excitation of free jets (Hussain & Zaman 1975), we found that the measured roll-up frequency was a function of the streamwise distance of the hot wire from the lip (i.e. the separation point). As the probe was traversed downstream within the free shear layer, the frequency progressively decreased, followed by jumps at intervals to higher values. Especially the latter feature, affirmed by repeated measurements, appeared inexplicable on the basis of any plausible shear-layer dynamics. Other authors have observed frequency dependence on x but attributed it to the Doppler effect or refraction effect of sound waves in the noise producing region (Winant & Browand 1974; Ko & Davies 1971; Ko & Kwan 1976). Neither of these effects could explain the apparent peculiarity of our data. Eventually, we established that the frequency variations observed by us were due to the edge tone effect of the hot-wire probe on the free shear layer.

1.2. *The edge-tone phenomenon*

When a thin slit jet impinges symmetrically on a plane wedge the resulting sound is called jet edge tone. The sound has interesting characteristics: the sound frequency spectrum has a strong peak; the peak frequency increases with decreasing jet–wedge distance h or with increasing jet speed U_e followed by positive jumps, the regions

between jumps being called 'stages'; there is a minimum value of h below which no edge tone occurs; for a fixed h there is a minimum U_e below which no edge tone occurs also; the interstage frequency jumps are associated with hysteresis, i.e. the jump frequencies depend on whether h or U_e is increased or decreased; etc.

The jet edge tone phenomenon was first reported by Sondhaus in 1854. Helmholtz, and Rayleigh, among others, also studied it, but it was Waschmuth who in 1904 first looked at edge tone in the absence of a resonator. His interpretation was that the jet acted as a flexible rod pendulating on impact on the wedge and that the noise radiated from the wedge rather than the jet, probably owing to vibration of the wedge. Benton in 1912 demonstrated that wedge vibration was not necessary for edge tone production. Schmidtke in 1919 postulated the presence of Kármán vortex streets along the sides of a wedge in stage I and between the jet and wedge in higher stages. Kruger, in 1920, was the first to try to explain the frequency jump as the consequence of the condition that the jet–wedge distance h be a multiple of the most unstable mode wavelength λ of the jet. He also suggested that a compression wave travels back to the jet exit to maintain a self-sustained edge tone; this acoustic feedback concept was presumably shown to be erroneous by Richardson (1931), who also inferred from his data that h/λ = stage of the edge tone. Brown (1937*a*) made a careful smoke visualization to provide probably the most comprehensive documentation yet of the jet edge tone flow, and derived the empirical (dimensional) formula for the edge tone frequency f,

$$f = 0{\cdot}466j(U_e - 40)[(1/h) - 0{\cdot}07], \tag{1}$$

where $j = 1$, 2·3, 3·8, 5·4 in stages I, II, III and IV; U_e is the exit velocity and h the jet–wedge distance (in c.g.s. units). Brown concluded that the stage I can occur simultaneously with any of the other stages. In his second paper, Brown (1937*b*) emphasized the superficiality of the existing interpretations of the edge-tone mechanism and argued that at low speeds the jet disturbance caused by the wedge was the controlling factor while at high speeds acoustic feedback from the wedge produced the edge tone.

Curle (1953) extended Kruger's and Richardson's ideas by postulating that the instability of the jet produces its pendulation, which in turn triggers separation vortices alternately on the two sides of the wedge. The circulation associated with these vortices induces coherent embryonic vortex formation back at the jet exit; these vortices then grow owing to jet instability, thus providing the stable feedback. He rejected the role of fluid compressibility, and based on Brown's (1937*a*) data he argued that the h–λ relation, for the (integral) stage J of the edge tone, should be

$$h/\lambda = (J + \tfrac{1}{4}). \tag{2}$$

Nyborg (1954) developed a dynamical theory by assuming that the jet consisted of a streak of discrete particles under the action of a uniformly distributed transverse force field. The central hypothesis is that the transverse acceleration of each particle depends only on its distance from the jet exit and its instantaneous transverse displacement. The resulting integral equation for the jet displacement, even for simple choices of trial functions for the integrand, produced self-sustained oscillation solutions with realistic frequency variations and jet trajectories. This over-simplified theory, however, fails to predict when the frequency jumps will occur, and why there should be a lower limit of h for the existence of edge tone.

Powell (1961) considered the edge tone phenomenon to consist of four simultaneous effects, the net transfer function for the stable feedback system being the product of the effectiveness of each. Each effect is represented as a complex gain factor having an amplitude and a phase change; for the case of stable self-excitation the total gain must be unity and the total phase change an integral multiple of 2π. Recognizing the complexity of the jet flow field, Powell used the Brown–Curle relation (2) as an independent criterion to account for the flow field's part in the feedback control loop. He then developed a nonlinear gain criterion to explain the existence of the lower limit of the jet–wedge distance for edge tone production. This theory also explained multiple tones, frequency jumps and frequency hysteresis.

Curle's hydrodynamic theory assumes that the vortex generated on each side of the wedge by the jet instantaneously triggers an embryonic vortex at the lip on the same side but of opposite sign. Nyborg's theory, however, is totally devoid of the flow physics and its limited success would appear to be fortuitous. Powell's theory differs from Curle's in that the feedback in the former is acoustic while it is hydrodynamic in the latter. Powell's theory has been regarded as probably the most rigorous. However, the $n+\frac{1}{4}$ wavelength criterion used by Powell is arbitrary. The cornerstone of Powell's theory is the nonlinearity of jet disturbance while it can be argued that at least for the first stage the nonlinearity may not be large. In spite of sustained efforts by these leading researchers, the jet edge tone theory is still unsatisfactory, indicating incomplete understanding of the phenomenon.

Woolley & Karamcheti (1974) have attempted to show through their quasi-parallel flow instability computations that the non-parallel nature of jet flow can explain most edge tone characteristics.

1.3. *Motivation and objective*

After coming across the free shear layer tone phenomenon, we failed to find any previous study of this phenomenon in the literature. The instability characteristic of these shear layers (Michalke 1965, 1972; Freymuth 1966; Hussain & Thompson 1975) associated with a top-hat velocity profile at the jet exit are different from those of the slit jets with parabolic exit profiles (Sato 1960) used in conventional edge tone studies (Karamcheti *et al.* 1969). In the jet–wedge edge tone, the jet impinges on the wedge symmetrically; there is lack of such symmetry in the shear layer tone. While Curle's (1953) hydrodynamic theory is based on the symmetric vortex patterns on the two sides of a jet triggering vortices of opposite sign on the two sides of a wedge, the rolled-up vortices in a mixing layer are of one sign only. This suggested that the edge tone characteristics in a single free shear layer would be different from those in a slit jet; hence the motivation for this study. As we shall see, the shear layer tone has some similarities with the jet edge tone as well as some differences. Our detailed hot-wire measurements not only document this phenomenon but also shed further light on the jet edge tone phenomenon itself.

There are numerous practical applications where the shear layer tone is of interest: these range from whistles; to holes in transonic tunnel walls; to cavities in various kinds of wind tunnels, in rocket motors, and in continuous lasers; to open cavities on flight vehicles, ships and submarines. In some of these, the shear layer tone phenomenon can produce excessive noise or structural vibrations or heat transfer or drag. In the presence of a cavity, the shear layer tone is coupled with the cavity resonance;

the free shear layer tone is not influenced by any such cavity resonance. To our knowledge, this is the first study of the *free* shear layer tone phenomenon.

After the completion of this work, we became aware of two independent, contemporary investigations (Bolton 1976; Sarohia 1977) of oscillation in flows over cavities. Bolton (1976) has studied the excitation of a Helmholtz resonator jacket covering a circular orifice (cutout) in a turbulent pipe flow and inferred that the feedback across the cut-out is hydrodynamic. Sarohia (1977) has studied oscillation of laminar flows over cavities on slender axisymmetric bodies. Even though his study shows that the data are independent of cavity depth below a certain size, the acoustic modes and hydrodynamics in the cavity obviously play a significant role. Furthermore, his study is inherently different from ours, the former being influenced by multiple length scales associated with the slotted slender body. In spite of the configuration differences, the hot-wire based data of Sarohia provide some details of the local shear layer oscillations; these data will be compared with ours whenever appropriate.

2. Experimental apparatus and procedures

The experiments were carried out in the free shear layers of a plane and a circular air jet facility, briefly described by Hussain & Clark (1977) and Hussain & Zaman (1975), respectively. A 2·54 cm diameter nozzle follows the 25·4 cm diameter settling chamber in the circular jet facility; the 140 cm × 3·18 cm plane jet follows the 140 cm × 140 cm settling chamber. Both flows exit through perpendicular end plates and discharge in a large laboratory with controlled temperature, humidity and traffic. Data were obtained by standard hot-wire techniques employing constant-temperature (DISA) anemometers and 0·2 cm tungsten hot wires of 4 μm diameter.

The hot wire traverses in streamwise (x), transverse (y), and spanwise (z) directions and yaw (α) were carried out through the action of stepping motors with resolutions of 0·00254 cm and 0·01°, respectively, under remote manual and computer controls. Integral measures of the shear layer were obtained on-line with our laboratory minicomputer (HP 2100). A Spectrascope SD335 real-time spectrum analyser (with a maximum range of 0–50 kHz in 500 frequency lines) was used to obtain the spectra of the velocity signals; unless otherwise stated, each spectrum is an ensemble average of 128 successive realizations. The spectrum is displayed on the built-in scope and the amplitudes and frequencies of the spectral peaks were read directly with the help of a cursor to within $\pm$ 0·1 % full scale. Spectra presented refer to a one-dimensional longitudinal velocity frequency spectrum $S_u(f)$ defined such that $\int_0^\infty S_u^2(f)\,df = \overline{u}^2$. A PAR 129A lock-in-amplifier was used to measure the amplitudes and phase variations of the shear tone induced velocity fundamental.

For all measurements reported in this paper, the initial boundary layer was laminar. The boundary layer at 0·3 cm before the lip (i.e. the separation point) was carefully traversed with the hot wire to record mean velocity and longitudinal fluctuation intensity profiles. The velocity fluctuations in this boundary layer were observed to be of fairly low frequency both by scope trace check and by spectral analysis; these can be traced to either settling chamber cavity resonance frequencies or blower blade frequency. The fluctuation intensity profile was consistent with that of a time-dependent laminar boundary layer (Hussain & Clark 1977). The mean velocity profile

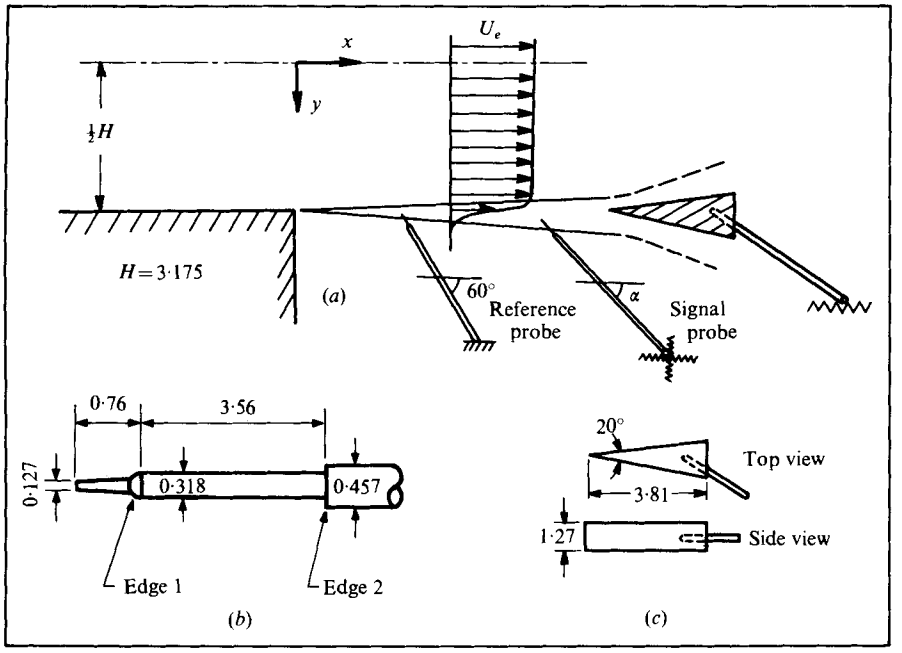

FIGURE 1. (*a*) Schematic of the free shear layer, wedge and hot-wire probe arrangement; (*b*) hot-wire probe tip details; (*c*) wedge details. Dimensions are in cm.

shape factor was very close to the flat-plate laminar boundary-layer (Blasius profile) value of 2·59. Considering all these factors, we considered the initial condition to be laminar.

Figure 1 (*a*) shows schematically the flow and the probe orientation in the flow; the detailed geometry of the hot-wire probe used is shown in figure 1 (*b*). A 1·27 cm wide and 3·81 cm long, 20° sharp wedge (figure 1 *c*) was used to study the basic physics of the free shear-layer tone.

Unless otherwise stated, all single probe data were taken with the probe (acting as the wedge) inclined at an angle α of 20° with the x axis (figure 1 *a*). Most of the data reported here pertain to the plane free shear layer of a plane jet with top-hat velocity profile, within one gap-width downstream. Note that the jet exit centre has been conveniently chosen as the origin of the co-ordinates. Also note that while the streamwise distance of the velocity measurement point is denoted by x, the distance of the wedge-tip from the exit plane (lip) is denoted by h.

3. Results and discussion

3.1. *Free shear layer tone induced by a hot-wire probe*

3.1.1. *Frequency variation with the lip–probe distance.* Figure 2 shows the one-dimensional frequency spectra of the longitudinal velocity fluctuation u determined by the hot wire placed at different axial locations x in the plane free shear layer. Only the single-wire probe as sketched in figure 1 (*b*) was in the flow at the y location where $U/U_e = 0{\cdot}95$ (with $\alpha = 20°$). With increasing hot-wire distance x from the lip,

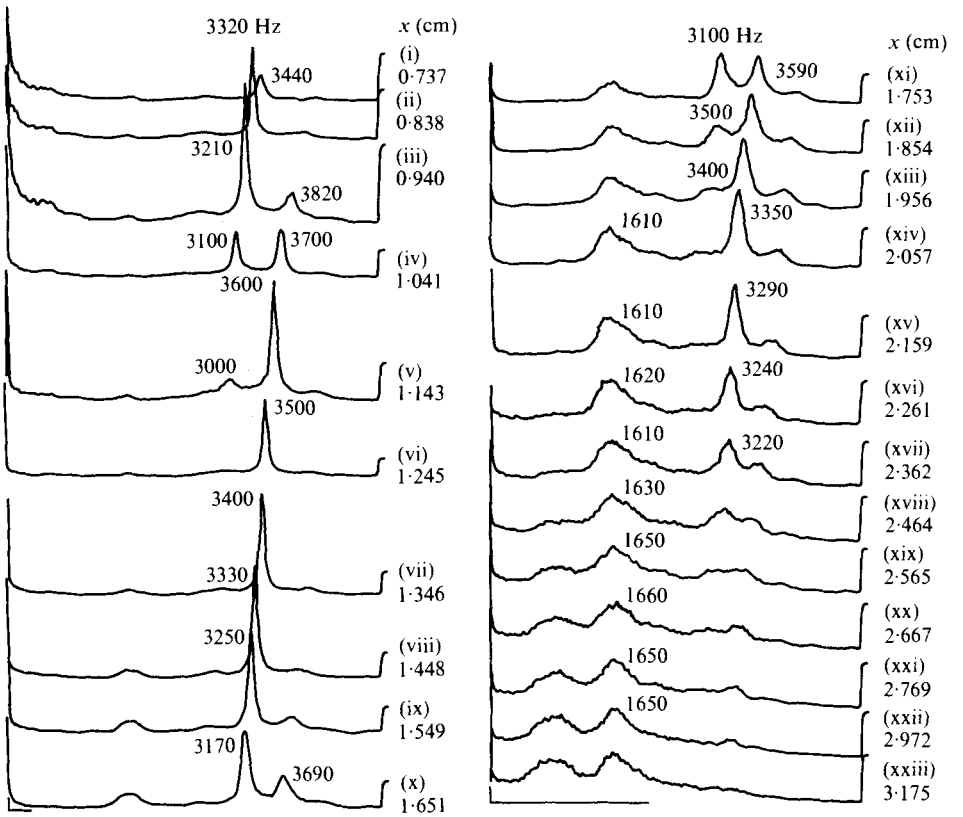

FIGURE 2. Longitudinal one-dimensional frequency spectrum $S_u(f)$ of the signal from the hot-wire probe placed at different axial locations x in the plane free shear layer; $U_e = 37{\cdot}2$ m/s. Hot-wire placed at the y location where $U/U_e \simeq 0{\cdot}95$. Plots are on linear–linear scales; abscissa range for all the traces is 0–5 kHz. Traces (vi)–(xxiii) have an identical vertical scale; with respect to this, the vertical scales for traces (i)–(iii) are magnified by a factor of 10 and those for traces (iv)–(v) by $10^{\frac{1}{2}}$.

the frequency decreases; in stage I, the spectral peaks, discernible for $x \gtrsim 0{\cdot}33$ cm, are of very low amplitudes and thus not shown. Figure 2 shows that the amplitude increases with x and reaches a maximum at $x \simeq 0{\cdot}94$ cm (in stage II) before decreasing with increasing x. At $x \simeq 0{\cdot}94$ cm another peak at a higher frequency (i.e. stage III) appears in the frequency spectrum. With further increases in x, the amplitude of the second mode in this bimodal region continues to grow while that of the first decreases, the frequencies of both, of course, decreasing progressively. The sequence of events repeats at larger x. After the fourth stage a subharmonic frequency appears, which overtakes the fourth stage in amplitude at $x \simeq 2{\cdot}46$ cm.

The peaks in the velocity spectrum gradually disappear further downstream; the energy becomes distributed in frequency with gradual roll-off at higher frequencies, indicating progressive spectral broadening and randomization of flow fluctuations due to the evolving turbulence through the (nonlinear) cascade process.

The variation of the spectral peak frequency in the transverse direction was checked and found to remain essentially unchanged across the shear layer width for a number of x stations. Constancy of the spectral peak frequency in y rendered subsequent

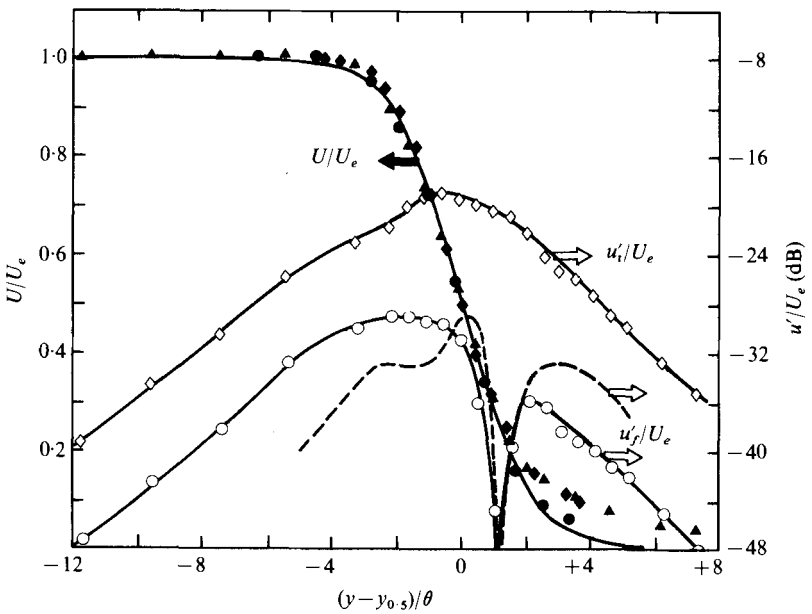

FIGURE 3. Variation of the longitudinal velocity U, total turbulence intensity u_t' and the shear layer tone fundamental (r.m.s.) amplitude u_f' as functions of normalized transverse distance y from the half-mean velocity point for the plane free shear layer at $U_e = 37{\cdot}2$ m/s. Mean velocity at: ●, $x = 0{\cdot}25$ cm; ▲, $x = 1{\cdot}35$ cm; ◆, $x = 3{\cdot}18$ cm; solid line through these data is the profile $U/U_e = 0{\cdot}5 - 0{\cdot}5\tanh((y-y_{0\cdot5})/2\theta)$. –◇–, u_t'/U_e profile at $x = 1{\cdot}35$ cm. u_f'/U_e profile at $x = 1{\cdot}35$ cm: –○–, data; – – –, spatial stability theory (Michalke 1965).

measurements easier because the transverse position of the probe or the wedge in the shear layer was not critical as far as frequency measurement was concerned.

Figure 3 shows the longitudinal mean velocity distributions across the plane free shear layer for $U_e = 37{\cdot}2$ m/s at three streamwise stations. The antisymmetric profile $U/U_e = 0{\cdot}5 - 0{\cdot}5\tanh((y-y_{0\cdot5})/2\theta)$, used by Michalke (1965) and Freymuth (1966) for spatial stability calculations, is also plotted for comparison. The departure from antisymmetry of the plane free shear layer velocity profile was also observed by other investigators (Liepmann & Laufer 1947; Hussain & Thompson 1975). Especially, the lack of agreement of the data with the tanh-profile at the low-speed side can be attributed to a number of factors: large hot-wire errors at low velocities due to large fluctuation intensities and the transverse velocity, and the inherent changes in the profile due to its being in a state of relaxation from the boundary layer to the free shear layer profile.

Note that if U/U_e were plotted as a function of $y - y_{0\cdot5}$ non-dimensionalized by the shear layer vorticity thickness

$$\delta_\omega = U_e/(\partial U/\partial y)_{\max} = \left[\int_{-\infty}^{\infty} |\omega| dy\right] \Big/ |\omega|_{\max},$$

a better congruence of the mean velocity profiles would be obtained (Hussain & Thompson 1975). Since the instability of the shear layer is sensitive to the profile details near the location of mean vorticity maximum (at $U/U_e = 0{\cdot}5$), the vorticity thickness δ_ω, being determined by the profile at that location, is a more appropriate length scale than an integral length scale like the momentum thickness θ. However,

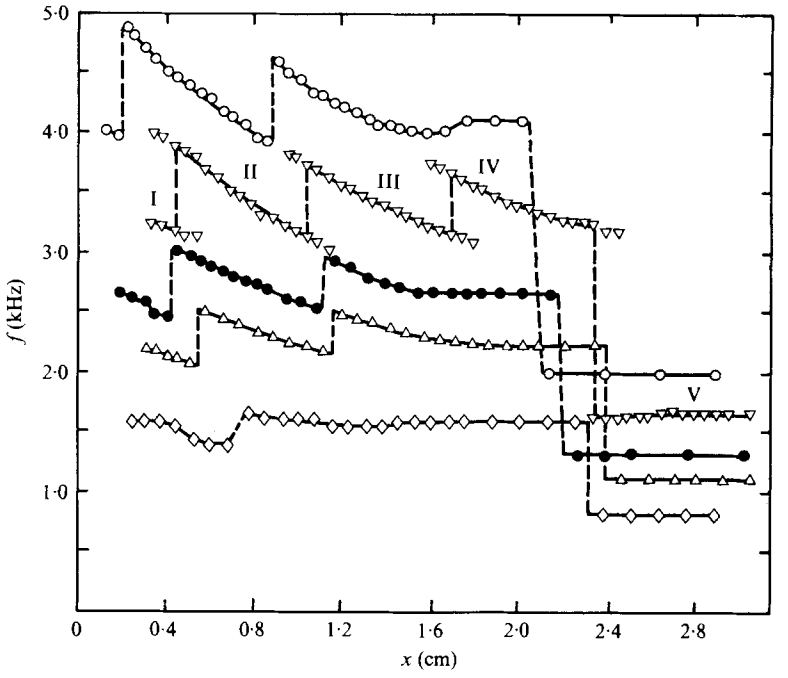

FIGURE 4. Axial variation of the probe-induced instability frequency of the plane free shear layer at different U_e: ○, 43·3 m/s; ▽, 37·2 m/s; ●, 32·0 m/s; △, 28·7 m/s; ◇, 21·6 m/s. For $U_e = 37{\cdot}2$ m/s, the stages of the shear layer tone are indicated.

owing to differentiation of discrete data across a very thin layer, δ_ω would have a larger uncertainty. For this reason as well as because of its widespread use by researchers in shear layers, the momentum thickness θ has been used as the length scale in figure 3. The r.m.s. total fluctuation intensity profile at $x = 1{\cdot}35$ cm is also shown in this figure; note that the peak of the intensity u'/U_e occurs at the location of maximum of slope $(\partial U/dy)$, where fluctuation production $-\rho\overline{uv}\,\partial U/\partial y$ will be the highest.

The fundamental r.m.s. amplitude profile $u'_f(y)/U_e$ at $x = 1{\cdot}35$ cm is also shown in figure 3; the minimum amplitude is consistent with the Kelvin's cat's-eye type flow associated with the motion of a vortex train over the hot wire. The theoretically predicted amplitude variation according to the spatial theory of Michalke (1965) is also shown for comparison. The agreement on the location of zero amplitude is impressive; however, the amplitude variations away from this location do not agree. Similar data by Freymuth (1966), and Hussain & Thompson (1975) showed much closer agreement of the amplitude data with the theory, but the Strouhal numbers used by them were much lower.

The disagreement between the data and the theoretical predictions could be due to a variety of factors: the mean velocity profile does not agree with the tanh-profile used in the theory; the flow is not parallel; there is a noticeable level of free-stream turbulence $u'_e/U_e = 0{\cdot}003$; the theory is for infinitesimal (linear) disturbances while the velocity fluctuations involved in the shear layer tone are indeed large-amplitude (nonlinear). Another factor which will introduce some artifact in the data is inherent in the method of acquisition of these data. The probe, acting as the wedge, was also traversed in y in order to take the data. While this does not introduce any shift in

frequency or wavelength, it would affect the measured amplitude distribution somewhat.

The fact that hot wires, as well as Pitot probes, have been used in free shear layers in many investigations and that no previous investigator has reported probe-induced edge tone effect, which can significantly alter not only the instability frequency but also integral measures of the shear layer, prompted us to document the effect further. The frequencies of the spectral peaks (similar to those shown in figure 2) as the probe is moved downstream along the line with $U/U_e = 0{\cdot}95$ in the plane free shear layer at five speeds, including the $U_e = 37{\cdot}2$ m/s case of figure 2, are shown in figure 4 as a function of the axial distance x of the hot wire. Note that around each frequency jump, there is an overlap region in which two spectral peaks occur. The overlap regions for the $U_e = 37{\cdot}2$ m/s case have been extended on either side of each jump (figure 4) as long as the smaller frequency spike could be distinguished from the background turbulence. For clarity, these overlaps for the other four speeds have not been shown; in each overlap (i.e. bimodal) region, the mode that has the higher amplitude of the two was chosen, thus defining an unambiguous jump frequency. Note also that with decreasing speed, the shear tone effect becomes irregular (discussed later).

The Roman numerals on this plot, shown only for the $U_e = 37{\cdot}2$ m/s case, indicate the stage of the tone, consistent with the nomenclature introduced by Brown (1937*a*). Data on the lower right-hand side of the plot (stage V) represent the subharmonic frequencies. The subharmonic amplitude gradually decreases with increasing x until it is submerged in the evolving background turbulence.

(*a*) *Subharmonic frequency.* No jet edge tone study has reported subharmonic formation. The occurrence of the subharmonic frequency observed in this study at all speeds is consistent with the phenomenon of vortex coalescence, which has been the subject of extensive, recent research (Winant & Browand 1974; Brown & Roshko 1974; Hussain & Zaman 1975, 1977; Browand & Weidman 1976; Zaman & Hussain 1977). A shear layer undergoes inviscid instability owing to the inflexional profile; the disturbance grows downstream, saturates by nonlinearity and the flow rolls up into spanwise vortex rolls. Such a vortex row is unstable (Lamb 1945); any non-uniformity in the spacings or strengths of two (or three) adjacent vortices cause them to coalesce (pair up) and form a larger vortex. Even though the details of the phenomenon of pairing is not yet well understood (Moore & Saffman 1975; Corcos & Sherman 1976; Roshko 1976; Zaman & Hussain 1977), it appears that interactions like coalescence of large-scale coherent structures play the key role in the evolution of these structures in free shear layers as well as jets, wakes and even, turbulent boundary layers.

It is remarkable that the organization of the flow due to edge tone feedback brings out the subharmonics associated with vortex coalescence which otherwise would occur randomly in space and time and thus would not be clearly discernible from the velocity spectrum in a free shear layer without any edge or external excitation. After the occurrence of the first subharmonic starting at $x \simeq 1{\cdot}5$ cm in figure 2, note that another (broader) peak at half this subharmonic frequency arises at $x \simeq 2{\cdot}5$ cm, suggesting a second stage of vortex coalescence. The occurrence of the vortex pairing (or tearing) ahead of the wedge would imply that only the coalesced vortices impinge on the wedge and thus provide feedback at the lip only at alternate periods of the shear layer unstable mode. Such alternate feedback, along with the fact that the

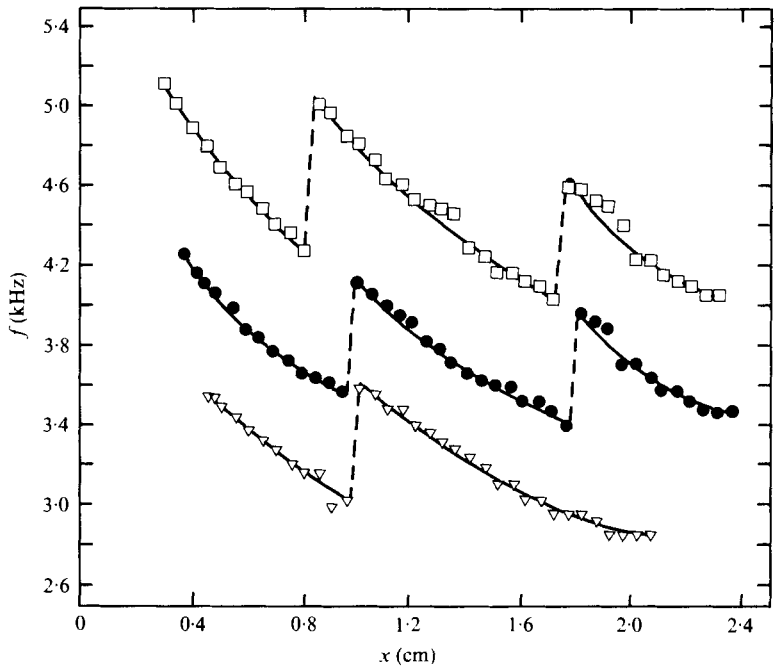

FIGURE 5. Axial variation of the probe-induced instability frequency for the axisymmetric free shear layer at different U_e: □, 46·0 m/s; ●, 40·2 m/s; ▽, 36·7 m/s.

subharmonic occurs at large lip–wedge distances h, would suggest that the effect of the feedback at the lip would be inherently weak, and thus would produce some jitter in the location of its nonlinear saturation and roll-up, as well as in periods of impingement on the wedge. This would explain why the peaks at the subharmonic frequencies in figure 2 are weak and broadband. We have shown in separate studies (Hussain & Zaman 1975, 1977) by both hot-wire measurements and flow visualization that vortex pairing, which otherwise occurs randomly in space and time, can be organized and accentuated by controlled excitation at appropriate Strouhal numbers. Specifically, in the 'shear layer mode', the pairing occurs at a Strouhal number $St_{\theta e} \simeq 0{\cdot}011$. The present study shows that the fundamental Strouhal number, $St_{\theta e} = 2f_v\,\theta_e/U_e$, for the shear layer under tone to produce subharmonics is about 0·0118; f_v is the subharmonic frequency in stage V in figure 4. This lends further credence to the view that stage V is due to vortex coalescence in the 'shear layer mode'.

(*b*) *Axisymmetric free shear layer.* To further confirm that the hot-wire probe produced the shear-layer tone, similar hot-wire spectra measurements were taken in the free shear layer of a 2·54 cm diameter circular jet at three speeds; the ratio D/θ_e being large, the curvature of the axisymmetric configuration should not be of any significance. Frequency *vs.* axial distance curves for three speeds are plotted in figure 5. Note that at the locations of jumps, overlap regions exist but the overlap frequencies have been omitted by following the same procedure as for figure 4; evidence of coalescence resulting in a subharmonic peak was also found in these data but has not been shown in this figure. As expected, all axisymmetric free shear layer tone data are similar to those in the plane mixing layer and thus are not shown further on.

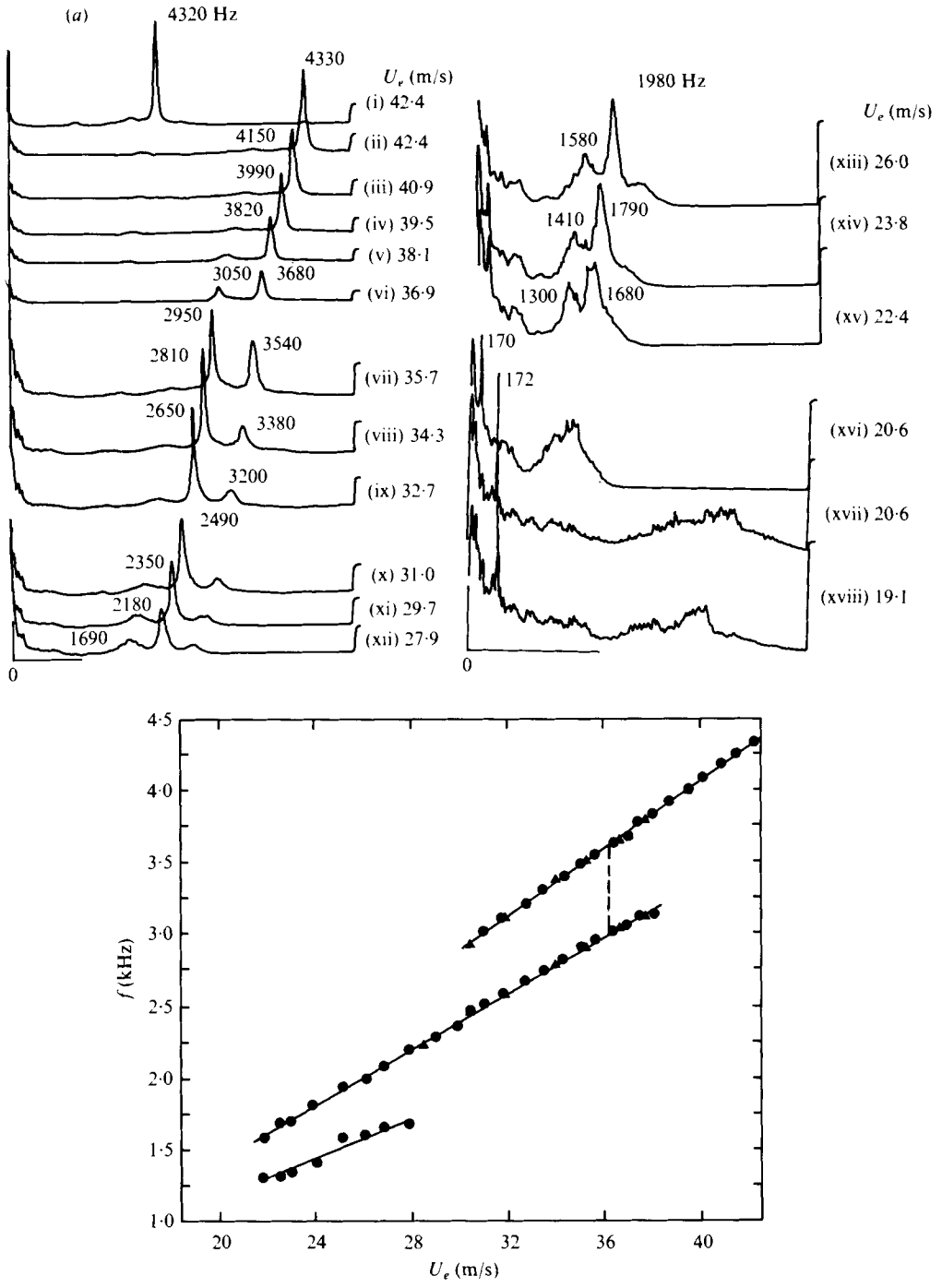

FIGURE 6. (*a*) Spectra $S_u(f)$ of the velocity signal in the plane free shear layer at different U_e. Hot wire was placed at $x = 1{\cdot}016$ cm; its transverse location was adjusted to keep it at $U/U_e \simeq 0{\cdot}95$. Plots are on linear–linear scales. Abscissa range is 0–10 kHz for trace (i), 0–2 kHz for traces (xvii) and (xviii), and 0–5 kHz for the rest. Vertical scales are arbitrary. (*b*) Variation of the plane free shear layer tone frequency with U_e for $x = 1{\cdot}016$ cm; circular data points are for increasing U_e and triangular data points for decreasing U_e.

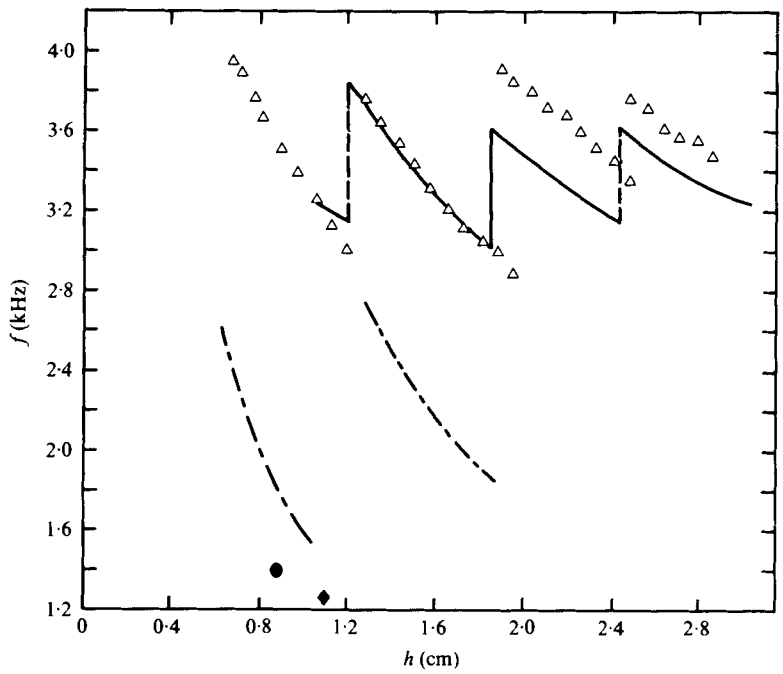

FIGURE 7. Variation of the plane free shear layer tone frequency with the axial distance h of the wedge; $U_e = 37{\cdot}2$ m/s. The solid lines represent data obtained with the probe only (figure 4), the probe distance having been corrected to represent the distance from the lip to edge 1 of the probe (figure 1*b*). – – –, equation (1); ◆, Sarohia's (1977) second stage data.

3.1.2. *Variation of frequency with jet exit speed.* Variation of the tone frequency f with U_e is shown with the help of u spectra plots in figure 6(*a*). Trace (i) of figure 6(*a*) confirms that there is no conspicuous spectral component other than the tone frequency while the last two traces show the details of the low-frequency spectral content. The discussion of the sequence of events with decreasing U_e is similar to that with increasing h (figure 2).

At lower speeds, the clear sharp spikes that characterized the spectra at higher speeds degenerate into a band of small-amplitude spectral components many of which could be attributed to the characteristics of the jet flow facility, such as the settling chamber resonance, the blower blade passage frequency (172 Hz), etc. These spectral peaks become comparatively significant at lower U_e and thus discouraged exploration of stage I at still lower U_e, as well as of the lowest speed $U_{e\min}$ that can produce shear tone, at each h. This facility constraint makes it difficult to identify tone frequencies at low U_e, a possible factor for irregular $f(x)$ data at low U_e (figure 4).

The probe-induced shear tone frequencies from figure 6(*a*) and from spectra at intermediate speeds are plotted in figure 6(*b*) as a function of exit speed U_e. The circles in figure 6(*b*) show data obtained when U_e was increased; the triangular data points were obtained with the speed decreasing. The vertical dashed line locates the jump from stage III to II, identified in the same way as for figure 4. The jump from stage II to I is not shown as the study could not be extended to still lower U_e, for reasons explained earlier.

3.1.3. *The effective wedge on the probe body.* Having discovered the principal symptoms

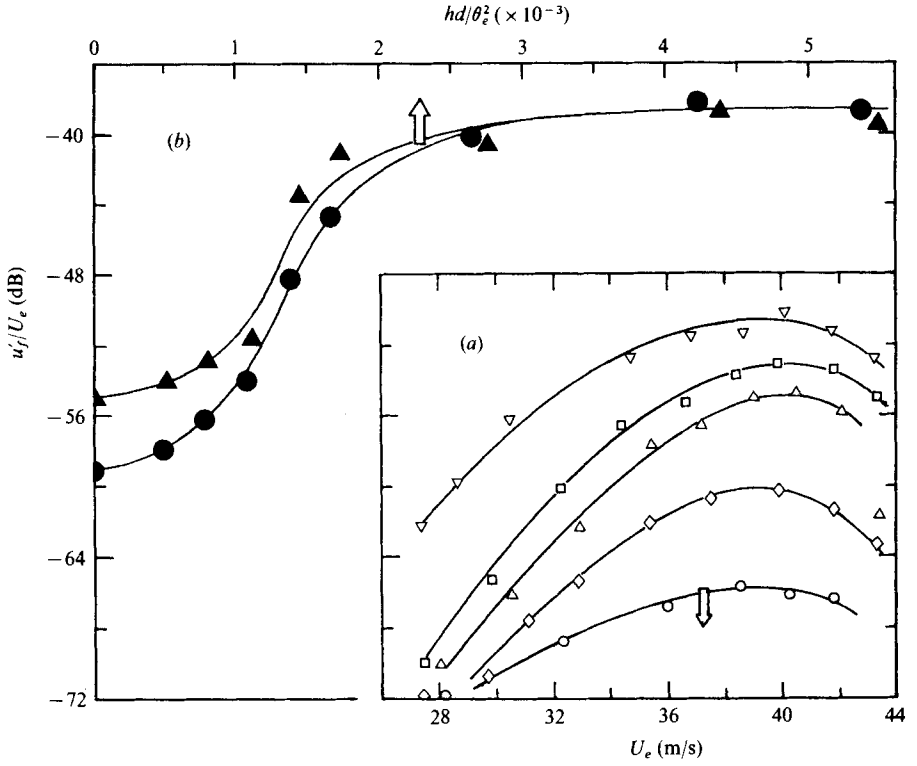

FIGURE 8. (*a*) Velocity fundamental amplitude u'_f/U_e as a function of speed U_e for cylinders of different diameters d: ▽, 0·635 cm; □, 0·315 cm; △, 0·198 cm; ◇, 0·165 cm; ○, 0·091 cm; hot wire located at $U/U_e = 0{\cdot}10$. (*b*) u'_f/U_e as a function of hd/θ_e^2: ▲, $U_e = 43{\cdot}3$ m/s, $h/\theta_e = 115$; ●, $U_e = 37{\cdot}2$ m/s, $h/\theta_e = 112$; hot wire located at $U/U_e = 0{\cdot}20$.

of the free shear layer tone, we wanted to determine the part of the probe support that acted as the effective wedge. From the sketch of the probe in figure 1 (*b*), edges 1 and 2 appeared possible candidates. We found that slight changes in the shape of edge 1, made by wrapping a cellophane tape around it, significantly changed the shear tone frequency while similar changes in edge 2 produced no effect. This strongly suggested that edge 1 on the probe support was acting as the wedge.

The location of the effective wedge on the probe was further confirmed by putting a 20° wedge in the flow (figure 1 *c*), and measuring the frequency variation of the resulting tone with axial distance h of the wedge. The frequency as a function of h (for the plane free shear layer at $U_e = 37{\cdot}2$ m/s) is plotted in figure 7; the hot wire was always at $U/U_e = 0{\cdot}20$ with $\alpha = 60°$ so that only small parts of the prongs were in the shear layer. The axial location of the hot wire was immaterial because for a fixed location of the wedge, the frequency was the same everywhere. The hot-wire probe induced shear layer tone data are replotted in figure 7 by shifting the data from figure 4 (for $U_e = 37{\cdot}2$ m/s) to the right by 0·737 cm, the length of the prongs, so that h now represented the distance of edge 1 from the lip. Probe induced shear tone data, thus shifted, agreed with the wedge data most closely (figure 7), confirming that edge 1 caused the shear tone.

However, the frequency variations in stages III and IV for the probe case and the

wedge case remain different. It was observed that the third and fourth stage tones for the wedge case were 'distorted' and the spectra contained noticeable higher harmonics of the shear tone fundamental frequency. In stages I and II, however, the velocity spectrum had a single, distinct peak. The differences between the frequency variations for the probe and the wedge in the third and fourth stages remain unexplained, the differences in the shapes and sizes of the two may be the reason.

Note that equation (1) based on the slit–jet edge tone does not represent the frequency variation in a shear tone as shown in figure 7. The data of Sarohia (1977) are also shown for comparison.

3.1.4. *Probe size effect.* The question naturally arises as to the effect of the probe size and orientation on the shear tone. Limited experimentation was undertaken on this question. Cylinders of different diameters d were held in the shear layer with the axis aligned with the downstream direction along the $U/U_e \simeq 0{\cdot}5$ line; the leading end of each cylinder was machined square to its axis. The tone induced velocity fundamental amplitudes u_f'/U_e as a function of U_e are shown in figure 8 (*a*) for different d. These data were taken with the cylinder held at fixed $h = 1{\cdot}6$ cm and the hot wire placed at the fixed location $x = 0{\cdot}5h$, $U/U_e = 0{\cdot}10$ and $\alpha = 60°$. All the data in this figure correspond to stage II of the shear layer tone. Clearly, the tone strength increases with cylinder diameter. Since tone induced velocity amplitude should also be a function of both h and θ_e, it appears reasonable to arrive at a size criterion by plotting u_f'/U_e as a function of hd/θ_e^2. Such a plot is shown in figure 8 (*b*) for two speeds; the corresponding values were chosen such that the tone in each case was in stage II and produced the largest velocity amplitudes u_f'/U_e. Even though the length scales are combined as hd/θ_e^2, h/θ_e being nearly the same, i.e. 112 and 115, this figure essentially gives the dependence of u_f'/U_e on d/θ_e.

Figure 8 (*b*) shows that the shear tone velocity amplitude increases rapidly with d above $d \simeq 5\theta_e$, reaching a maximum at $d \simeq 20\theta_e$, above which the amplitude is essentially independent of d. However, for very large diameters, i.e. for $d \gtrsim 50\theta_e$, the flow upstream was observed to be grossly disturbed. (Note that data in figure 8 (*b*) were taken with the hot wire located at $U/U_e = 0{\cdot}20$, thus explaining the different u_f'/U_e for the two figures, 8 (*a*) and 8 (*b*).) For $d \lesssim 5\theta_e$ yaw of the cylinder did not increase the minimal upstream influence at these sizes. From the above, it would appear that cylinders of diameters below $5\theta_e$ are safe for avoiding free shear layer tone.

3.1.5. *The most sensitive disturbance frequency for a shear layer.* The sharp peaks in the hot-wire signal spectra disappear when the probe is moved to the outskirts of the shear layer. Figure 9 shows frequency spectra plots with the hot wire placed at the y location where $U/U_e \simeq 0{\cdot}10$, with $\alpha = 60°$, so that the front end of the probe stem did not intersect the shear layer. The diameters of the prongs being about $3{\cdot}5\theta_e$, the disturbance due to the prongs was insignificant. Although there is no sharp peak in these plots, there is an unambiguous hump in each, the peak frequency of which remains constant within an axial distance in which at least two tone stages (with sharp spectral peaks) would be found if the probe support were in the shear layer. The broadband humps can be explained by the argument that, although there is no controlled external disturbance, there exists the 'white' background noise from which disturbances with frequencies in the unstable band are picked up and appropriately amplified by the shear layer. The peak of these humps should represent the most sensitive frequency. Figure 9 thus shows that the plane free shear layer under study

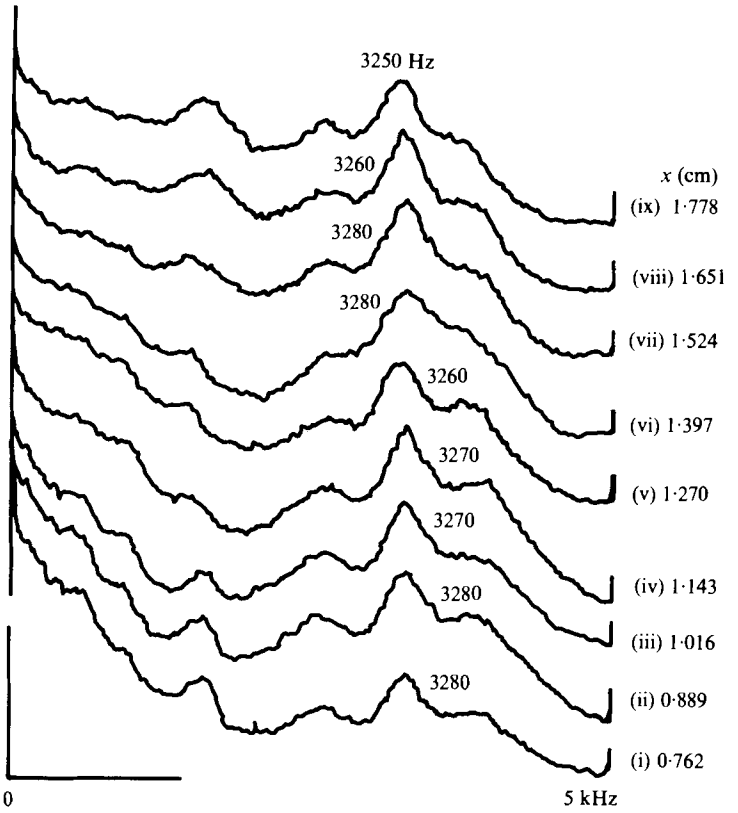

FIGURE 9. Spectra $S_u(f)$ of the velocity signal at different x in the plane free shear layer; $U_e = 37{\cdot}2$ m/s. Probe axis makes an angle of 60° with the jet axis and the transverse location of the hot wire at each x is adjusted to keep it at $U/U_e \simeq 0{\cdot}10$. Plots are on log–linear scales; abscissa range is 0–5 kHz and ordinates are arbitrary.

is most sensitive at about 3280 Hz when $U_e = 37{\cdot}2$ m/s. This frequency is also midway in any stage of shear tone frequency variation with x at $U_e = 37{\cdot}2$ m/s (figure 4). As shown in figure 2, the amplitude of the shear tone spectral component in any stage reaches its maximum near the middle of the stage. For $U_e = 37{\cdot}2$ m/s, maximum shear tone induced velocity amplitude was measured at $f = 3280$ Hz. Thus the amplitude of the shear tone is the largest when the tone frequency is the same as the most unstable frequency of the free shear layer.

We thus conclude that data on the sensitivity of shear layers to external disturbances should be obtained with the probe placed such that no sizable part of it intersects the shear layer. A sharp peak in the spectrum of the velocity signal from a hot wire in a thin shear layer should be interpreted with caution. The frequency of the probe induced tone may differ significantly from the natural roll-up frequency of the shear layer; note that the spectral peak frequency varies from about 2900 Hz to 3900 Hz for $U_e = 37{\cdot}2$ m/s depending on the probe location (figure 7) while the instability or natural roll-up frequency is 3280 Hz. The occurrence of a shear tone can also noticeably alter the mean shear layer characteristics as well as its coherent structure and thus its subsequent evolution. One way of avoiding shear tone would be, of course, to employ non-invasive measurements like laser-Doppler velocimetry; in this case, however,

apart from the space and price limitations, the large scatter volume would not provide shear layer data with fine spatial resolution. The probe induced shear tone itself, however, can be put to use in determining the most unstable frequency of the shear layer. This can be achieved by changing the probe position in x and identifying the location, and thus the tone frequency, at which the velocity fluctuation amplitude becomes largest.

3.2. *On the aspects of free shear layer tone phenomenon*

3.2.1. *Near-parallel shear flow theory.* The linear hydrodynamic stability theory for the propagation of small amplitude disturbances in a parallel shear flow predicts that the frequency of a normal mode experiencing the maximum amplification in a given shear layer is unique. However, owing to viscous diffusion of vorticity (i.e. laminar entrainment), free shear layers are not parallel; when the non-parallel effect is taken into account, a continuous decrease in the frequency of the most sensitive mode with increasing x is predicted (Woolley & Karamcheti 1974; Ling & Reynolds 1973). Clearly, the frequency of such an instability mode at any streamwise location scales with the local shear layer thickness, which can be characterized by the profile width $B = y_{0.95} - y_{0.1}$, or the momentum thickness

$$\theta = \int_{0.x}^{\infty} (U/U_e)(1 - U/U_e)\, dy$$

or the vorticity thickness δ_ω, each of which continuously increases downstream; $y_{0.95}$ and $y_{0.1}$ are the locations at which U/U_e is 0·95 and 0·1, respectively. Thus when either B or θ or δ_ω is used as the length scale, there should be a continuous decrease of the 'most unstable' frequency in the downstream direction.

Woolley & Karamcheti (1974) have shown that some of the main features observed in jet edge tone, such as decreasing frequency with increasing jet–wedge distance, can generally be explained by the non-parallel effect. However, they have not addressed a major feature of edge tone, namely the frequency jumps. If non-parallel flow theory were to explain the decrease in frequency with axial distance in edge tone, the local shear layer thickness would be the relevant length scale governing the instability mechanism, since the characteristic velocity scale U_e remains unchanged. Thus the Strouhal number based on B, θ or δ_ω should be expected to have a similar functional relationship in the different stages of edge tone operation. The following data clearly indicate that such is not the case.

For $U_e = 37{\cdot}2$ m/s, the streamwise variations of the plane free shear layer momentum thickness θ and vorticity thickness δ_ω were obtained from mean velocity profile traverses with the help of the on-line laboratory minicomputer. Figure 10 shows the variations of θ and δ_ω with x as obtained from the mean velocity profiles by traversing the single-wire probe only. In such measurements the effect of the transverse component of the mean velocity on the zero-speed side of the free shear layer introduces error. Instead of adopting any correction procedures – which are all questionable – to smooth out the zero-speed side tail of the mean velocity profile, we truncated the integration for θ at $U/U_e = 0{\cdot}1$. The vorticity thickness measured on the basis of the maximum slope of the mean velocity profile by least-squares fit of a straight line passing through four data points around the half mean velocity point is unaffected by this truncation. However, θ, being an integral quantity, exhibited much lower uncertainty compared with δ_ω; the uncertainty in the latter was $\pm 5\,\%$.

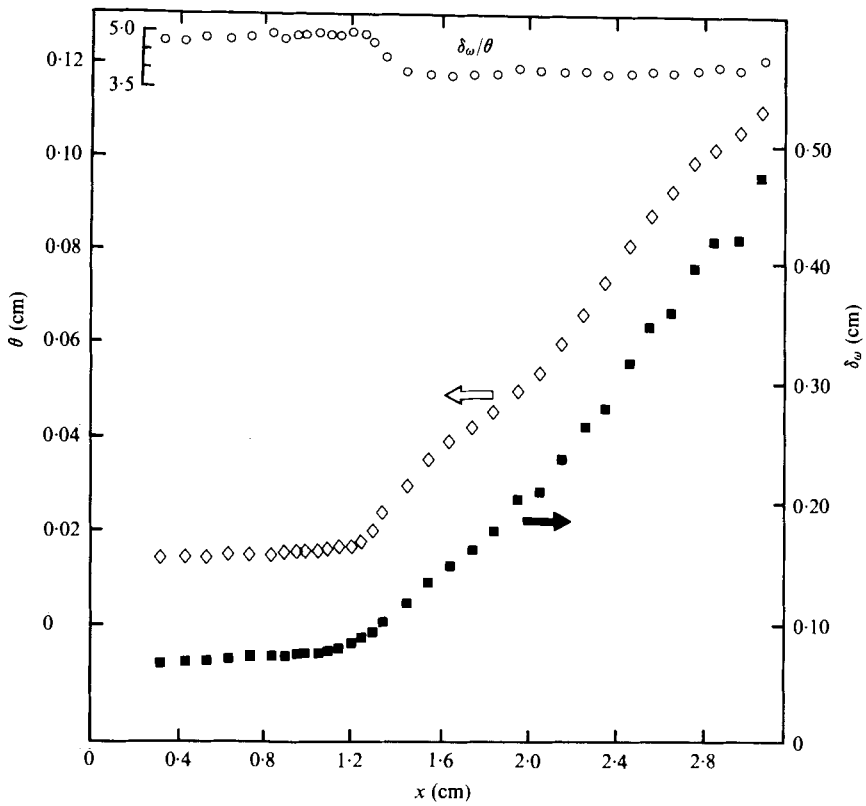

FIGURE 10. Variations with x of the momentum thickness θ, the vorticity thickness δ_ω and the shape factor δ_ω/θ of the plane free shear layer at $U_e = 37{\cdot}2$ m/s; ◇, θ; ■, δ_ω; ○, δ_ω/θ.

Also included in figure 10 is the streamwise evolution of the 'free shear layer shape factor' δ_ω/θ which has a value of about 5 for $x/\theta_c \leqslant 80$, but about 4 for larger values of x/θ_c. This abrupt change in δ_ω/θ (at $x \simeq 1{\cdot}2$ cm) should indicate an inherent change in the velocity profile, i.e. a sudden widening of the shear layer, and thus may indicate the location for roll-up of the free shear layer. The flow dynamics of the free shear layer before and after the roll-up are quite different; larger entrainment (i.e. entrapment) can be expected after roll-up. Since $d\theta/dx$ is the entrainment velocity divided by U_e, the higher $d\theta/dx$ beyond $x \simeq 1{\cdot}2$ cm in figure 10 does indeed suggest an inherent change in the shear layer structure and dynamics. We are studying further details through visualization. The oscillations in $\theta(x)$ indicate effects of successive stages of the tone on shear layer entrainment at 0·75 cm ahead of the wedge. The average value of $d\theta/dx = 0{\cdot}048$ is higher than Sarohia's (1977) values ranging up to 0·022. The value of $d\theta/dx$ in the self-preserving region of a shear layer was found to be 0·035 by Liepmann & Laufer (1947). Hussain & Zedan (1978*a*, *b*) found $d\theta/dx$ to vary over the range 0·028–0·035 depending on the initial condition. It is not unreasonable to expect a shear layer under tone to manifest a larger $d\theta/dx$ than the corresponding unperturbed free shear layer. This difference may also be partly due to the fact that $\theta(x)$ in figure 10 does not represent streamwise variation of θ in a particular shear layer under tone with a fixed wedge but successive $\theta(x)$ in front of the wedge as it is moved downstream. Further, the free shear layer adjacent to the lip here is far upstream

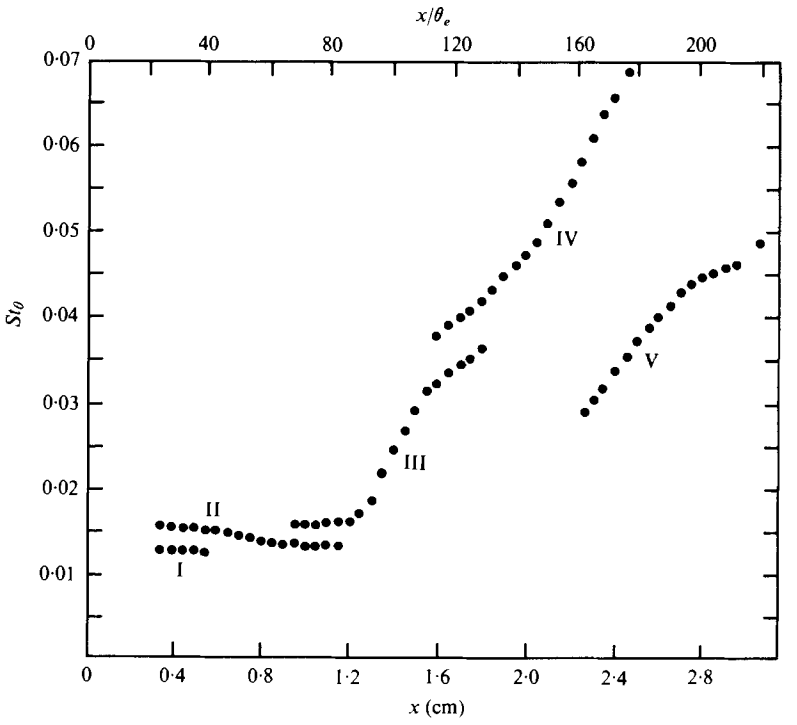

FIGURE 11. Strouhal number St_θ (based on local θ) *vs.* axial distance for the plane free shear layer at $U_e = 37{\cdot}2$ m/s. The stages indicated correspond to those in figure 4.

from the self-preserving region studied by Liepmann & Laufer (1947) and Hussain & Zedan (1978*a*, *b*).

The data of figure 10 coupled with the frequency data of figure 4 (for $U_e = 37{\cdot}2$ m/s) were used to obtain local Strouhal numbers based on θ and δ_ω. The variation of St_θ in the different stages is shown in figure 11. The plot of $St_{\delta\omega}$ *vs.* x is similar to that of St_θ *vs.* x and thus not shown.

Figure 11 shows that St_θ (and thus $St_{\delta\omega}$) does not remain constant in a stage. Its functional dependence on x is different in different stages; St_θ and $St_{\delta\omega}$ vary much less in the first two stages. These variations lead us to believe that the instability mechanism in free shear layer tone does not scale on its local characteristic length scale only and thus it would appear that near-parallel flow theories alone cannot explain the pattern of frequency variation even in one stage of operation. Other length scales such as the lip–wedge distance h, and time scales like h/U_e, vortex transit time from lip to wedge, disturbance feedback time from wedge to lip etc. must also be considered.

3.2.2. *The amplitude variation in the different stages.* All the following data pertain to the tone in the plane free shear layer created by the wedge as described before (figure 1). The audio tone produced by the wedge was much louder than that produced by the probe. The vortex formation at the tip of the wedge is two-dimensional and the vortex will be stronger for the wedge than for the probe. These, together with the fact that the wedge has a larger surface area would explain the louder tone produced by the wedge. The lip–wedge distance being much smaller than the sound wavelength,

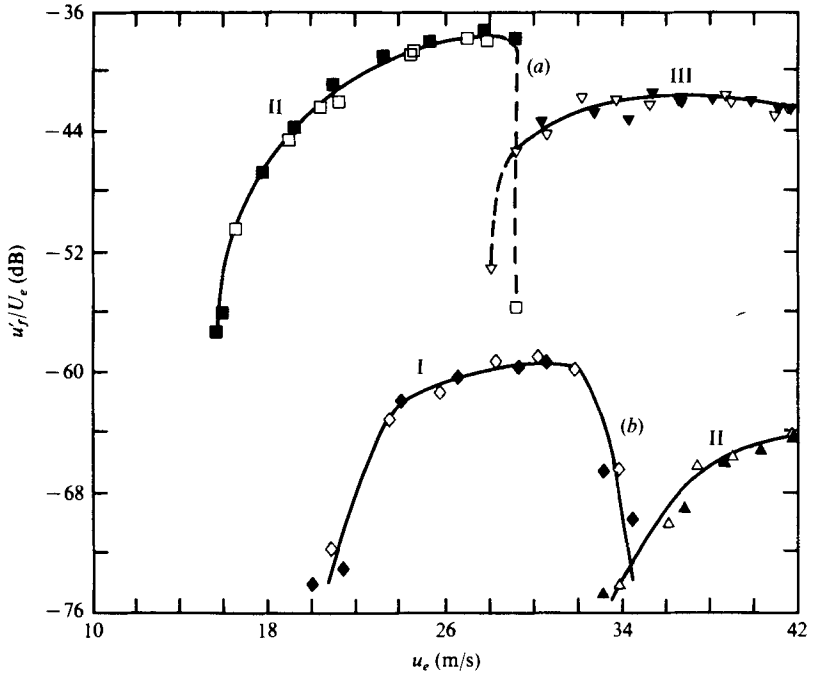

FIGURE 12. Variation of the r.m.s. amplitude of the plane free shear layer tone velocity fundamental with U_e. (*a*) Data obtained with wedge at $h = 1{\cdot}83$ cm; hot wire placed at $x = 1$ cm and $U/U_e \simeq 0{\cdot}95$ point. (*b*) Data with $h = 1{\cdot}22$ cm; hot wire placed at $x = 0{\cdot}63$ cm and $U/U_e \simeq 0{\cdot}95$ point. Solid data points were obtained while U_e was being decreased and the open ones while U_e was being increased.

the edge tone phenomenon is indeed a near-field effect and thus would depend on the shape and size of the wedge. The loudness of the tone was also extremely sensitive to the transverse location of the wedge in the free shear layer. The tone was loudest when the wedge was placed approximately at the half mean velocity point in the shear layer. Slight transverse displacement of the wedge from this point would make the audio tone strength drop drastically. The peaks in the u spectrum, however, could be clearly identified even when the tone could not be heard.

In the available literature on jet edge tone, hysteresis around frequency jumps had been observed to be a universal characteristic of the edge tone phenomenon (Brown 1937*a*; Curle 1953; Powell 1961; Karamcheti *et al.* 1969). That is, the transitions shown by the dotted lines in figure 4 and locations of frequency jumps in figure 6(*b*) would be different when the value of the independent variable – either h or U_e – is increased, as opposed to the case when it is decreased. In the probe-induced shear tone data, however, we could not find any evidence of hysteresis in the overlap regions; careful repeats confirmed this observation. Multiple modes as shown in figures 2 and 6(*a*) were not associated with hysteresis, i.e. the relative amplitudes remained the same whether the speed U_e was being increased or decreased. Figures 12 and 13 not only demonstrate the non-existence of hysteresis in shear layer tones produced by the wedge but also throw further light on the physics during the frequency jumps. For brevity, probe-induced tone velocity amplitude variations with h or U_e are not shown.

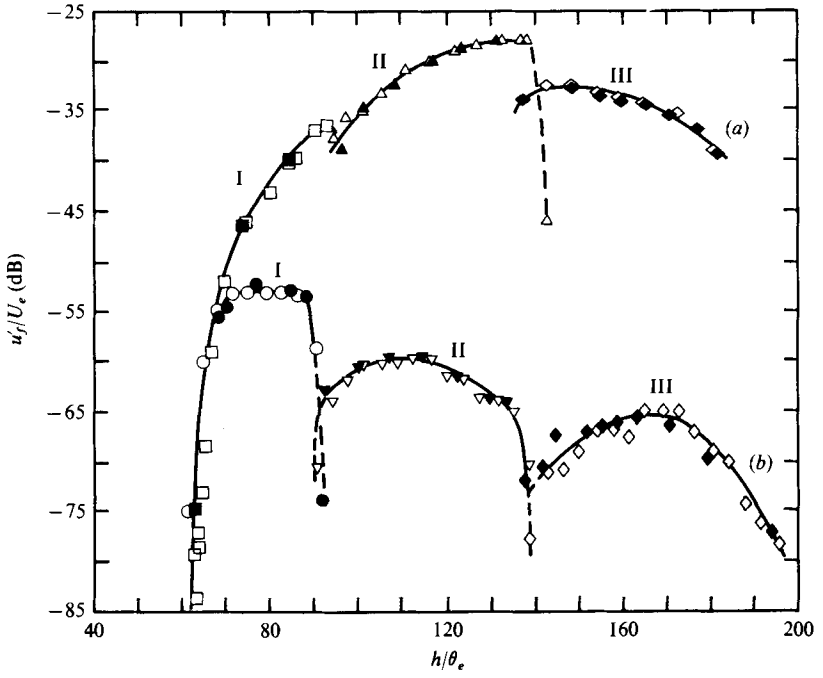

FIGURE 13. Variation of the r.m.s. amplitude of the plane shear tone velocity fundamental with axial distance h of the wedge: (*a*) the probe moved with the wedge, being held at a fixed distance 0·16 cm in front of the wedge; (*b*) the probe was fixed at a point (x = 0·25 cm and $U/U_e \simeq 0{\cdot}95$) in the flow. The solid data points were obtained while h was being decreased and the open ones while h was being increased.

The r.m.s. amplitudes of the shear layer tone spectral components as a function of the exit speed U_e for two wedge locations are presented in figure 12. The hot wire was placed between the lip and the wedge, at a fixed location (different for the two cases) and at $\alpha = 60°$ so that the probe body itself produced no interference. The solid data points in this plot represent those obtained while U_e was being increased and the open data points were obtained while U_e was being decreased, each run lasting about an hour. The stages indicated in the figure were determined from cross-plots of the associated frequency data as a function of the non-dimensionalized axial distance h/θ_e (see § 3.2.4).

Figure 12 shows that the amplitudes of the spectral components at any exit speed are functions of the lip–wedge distance h and, except for the unavoidable scatter in the data, are unique functions of the exit speed U_e itself, regardless of whether U_e was increased or decreased; thus no evidence of hysteresis was observed.

The differences between the amplitude distributions for the probe- and the wedge-induced velocity fluctuations provide interesting insight into the shear tone phenomenon. Unlike the case of the probe-induced tone, where the frequency overlap region covers a reasonably large range of U_e (figure 6*b*), the transition between the stages for the wedge case occurred rather abruptly and it was difficult to capture both spectral peaks simultaneously in the velocity spectra. This can be explained by the possibility that the sharp-edged plane wedge produces well-defined, stronger (smaller cross-section) vortices and produces a stronger sound (owing to larger surface area), so that

the feedback is stronger and there is less ambiguity in the selection of the tone wavelength or frequency. However, with very slow change in the velocity U_e we could obtain values of U_e at which two modes occurred intermittently and the resulting (128 ensemble averaged) spectrum exhibited the two peaks corresponding to the two stage frequencies. Careful observation of the scope trace revealed that the signal frequency changed intermittently from one value to the other, and that they never occurred simultaneously. Observations of the 'real time spectra' (i.e. single realizations of the frequency spectrum) clearly showed that the velocity spectrum had only one peak for each realization while a large ensemble average contained both the peaks. Our observation that the shear tone in the overlap region occurs in one mode only at a time contradicts other investigators' results that both modes in an overlap region of jet edge tone occur simultaneously (Brown 1937*a*; Powell 1961; Bilanin & Covert 1973; McCanless & Boone 1974). However, Sarohia's (1977) observation agrees with ours.

The amplitude distribution in the different stages of the shear tone as a function of axial distance h is shown in figure 13. The two sets of curves represent the following two cases: (*a*) the hot wire was placed at a fixed distance 0·16 cm ahead of the wedge and moved along with the wedge; (*b*) the hot wire was fixed in the flow at $x \simeq 0{\cdot}62$ cm and $U/U_e \simeq 0{\cdot}95$ while the wedge was traversed in x. Amplitudes for up to the third stage have been documented. In this figure, the solid data points represent those taken while h was being decreased and the open data points represent those while h was being increased, the run for each of the two cases lasting approximately an hour. The data for both forward and backward movement of the wedge, for both the cases shown, again follow the same smooth curves and no evidence of hysteresis could be found.

Powell's (1961) theory predicted that the hysteretic jumps in slit–wedge edge tone resulted from nonlinearity associated with the large amplitude fluctuations in the edge tone flow. During transition, a harmonic content in the established motion in a stage was presumed to provide stimulus for a jump to the next stage and a distinct jump thus occurring would 'more likely than not' be hysteretic. The non-occurrence of hysteresis in our study is currently being further investigated. Sarohia (1977) found no evidence of hysteresis in his configuration also.

The relatively higher amplitudes in figure 13(*a*) are due to the axial growth of the disturbances as the probe is moved in the axial direction. Note that amplitude variation in any stage in case (*a*) is not only due to the tone frequency falling near the most sensitive disturbance frequency (which receives maximum amplification) of the shear layer but also due to the fact that with increasing location x of the hot wire, disturbances are allowed to grow to larger amplitudes. Case (*b*), where the probe has been held at a fixed point in the flow field, thus more truly represents the growth and decay of the shear tone flow oscillation amplitude, depending on whether the tone frequency is approaching or receding from the most sensitive disturbance frequency of the free shear layer as the wedge is traversed in x. From the streamwise distribution of the shear layer tone induced amplitudes (not presented), we have found that the amplitude increases in x nearly exponentially, reaching its maximum at about $x = 0{\cdot}85h$ from the lip before decreasing again. This would explain why case (*b*) above should produce lower amplitudes (see figure 13).

As the wedge was moved upstream very close to the lip, the spectral peak component r.m.s. amplitude progressively decreased (the frequency, of course, changing simul-

taneously) until it became submerged in the background turbulence. Although the amplitude variation at the beginning of stage I in figure 13 is monotonic, the sharp drop in the amplitude (as h is decreased) indicates the existence of a minimum lip–wedge distance $h_{\min}$, at each U_e, for the tone to occur.

Likewise in figure 12, the inter-stage transitions in figure 13 occurred over a small distance unlike the case in probe induced edge tone (not shown). Even though the ensemble averaged spectrum showed peaks corresponding to both the stages during transition, careful scrutiny revealed that the edge tone occurred in only one mode at a time while intermittently switching between the two stages. It is to be noted that the subharmonic spectral peaks shown in connexion with the probe induced edge tone did not occur in a similar 'one or the other mode' with the fundamental edge tone component. The oscilloscope trace indicated that the signal constituted alternately stronger and weaker wave crests at the period of the fundamental thus producing the subharmonic spectral peak. A subharmonic in a spectrum in these situations has been shown to be associated with vortex coalescence (Zaman & Hussain 1977) and thus the generation of the subharmonic further downstream in the flow is due to vortex pairing in the free shear layer. Higher harmonics in the spectra of the wedge-induced tone velocity signal in stages III and IV resulted from the large-amplitude distorted wave form; these spectral peaks at higher frequencies have no physical significance.

3.2.3. *Spanwise extent of shear layer tone.* The presence of the 1·27 cm wide wedge in a plane free shear layer of 140 cm span raised the question as to whether the wedge was introducing instability over the entire span of the shear layer. Thus it was necessary to determine the spanwise extent of the wedge-induced shear layer tone. The hot wire was traversed in the spanwise direction at constant x and y keeping it at

$$U/U_e = 0{\cdot}20, \quad \alpha = 60°, \qquad \text{for} \qquad U_e = 37{\cdot}2\,\text{m/s}, \quad h = 1{\cdot}6\,\text{cm}.$$

The spectra of the velocity signal for different spanwise positions of the hot wire relative to the wedge were obtained. It was found that for a fixed wedge location, the tone frequency did not vary in the spanwise direction. The shear tone induced velocity amplitude decreases rapidly in z away from the wedge, reaching half and one-quarter of the peak value at $z = 2$ and 4 cm, respectively. The tone spectral peak is essentially lost at a distance $z = 10$ cm, which is considerably shorter than the 140 cm span of the plane free shear layer. Thus, the wedge did not precipitate instability of the shear layer over its entire span; the observed shear layer tone phenomenon is clearly a localized event.

3.2.4. *The characteristic length scales of the phenomenon.* The non-dimensional frequency $St_h (= fh/U_e)$ is plotted in figure 14 as a function of h for four different cases. For the two constant h cases, data obviously fall on vertical lines while for the other two cases, St_h can be found to increase nearly linearly with h. The shear layer tone data thus differ from the slit–wedge edge tone data of different investigations, where St_h has been observed to remain constant in each stage, the values being approximately 0·5, 1·1 and 1·7 in stages I, II and III, respectively (see Karamcheti *et al.* 1969).

The differences between the present data and the jet edge tone data are not unexpected because of the differences in the velocity profiles; the latter studies involved slit-jets with fully developed laminar channel flow (parabolic) profile at exit, while the plane free shear layer has an error function type profile (figure 3). The instability,

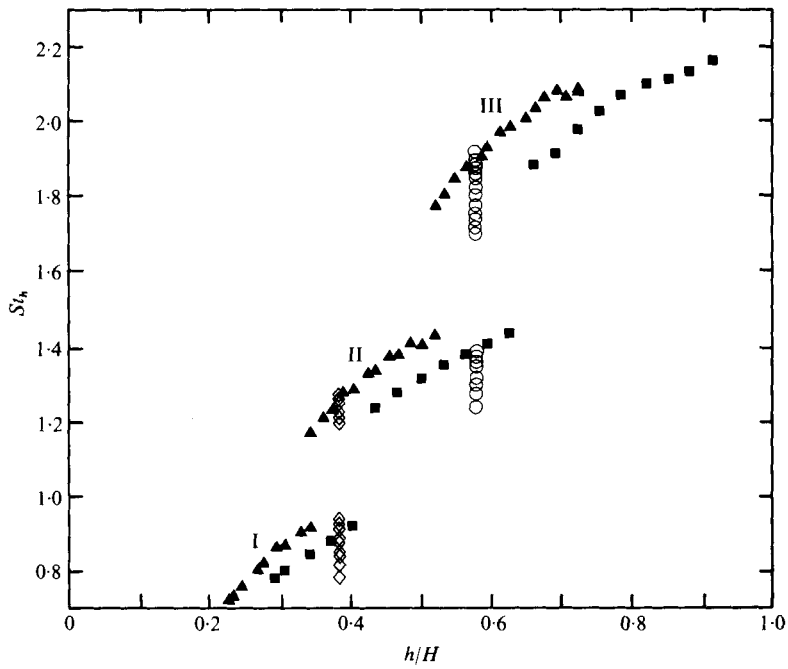

FIGURE 14. Strouhal number $St_h (= fh/U_e)$ of the wedge-induced plane free shear layer tone as a function of the lip–wedge distance h: ▲, variable h at $U_e = 43{\cdot}3$ m/s; ■, variable h at $U_e = 29{\cdot}3$ m/s; ◇, variable U_e with $h = 1{\cdot}22$ cm; ○, variable U_e with $h = 1{\cdot}83$ cm.

roll-up and the disturbance growth in x in the two cases are different. Apart from the imposed length scale h (the slit–wedge distance), the length scale associated with the instability mechanism for slit-jets is the slit width H, while such a configuration-imposed length scale does not exist in the free shear layer. Thus it is to be expected that the slit–wedge edge tone frequency variation data will collapse on the same horizontal line for a particular stage on a St_h *vs.* h/H plot; on the other hand, since H is no longer a length scale in a free layer tone, the differences between the different sets of data in figure 14 are to be expected. Figure 14 thus suggests the need for an appropriate length scale. Sarohia's (1977) data also show almost linear variation of St_h with h in each stage and agree qualitatively with ours.

For the free shear layer, the profile defines a length scale (θ or δ_ω) of its own. One can thus expect that if a characteristic initial shear layer thickness (e.g. θ_e) is chosen as the length scale, the free shear layer tone non-dimensional frequency variation for each stage may be universal. A number of data points for the exit shear layer momentum thickness (θ_e) as a function of the jet exit speed U_e were obtained. Least-squares fits of these points gave an appropriate θ_e *vs.* U_e curve, which was later used to obtain exit momentum thickness θ_e at any exit speed U_e.

The frequency (St_h) data of figure 14, when plotted as a function of h/θ_e, were found to fall on the same smooth line for each stage (figure 15*a*). These data also collapse on one another if plotted on a $St_{\theta e}$ *vs.* h/θ_e plot, as shown in figure 15(*b*). Note that the co-ordinates $St_{\theta e}$ *vs.* h/θ_e in figure 15(*b*) not only make the four sets of data collapse but also the ordinate variations in the three stages are brought in the same range.

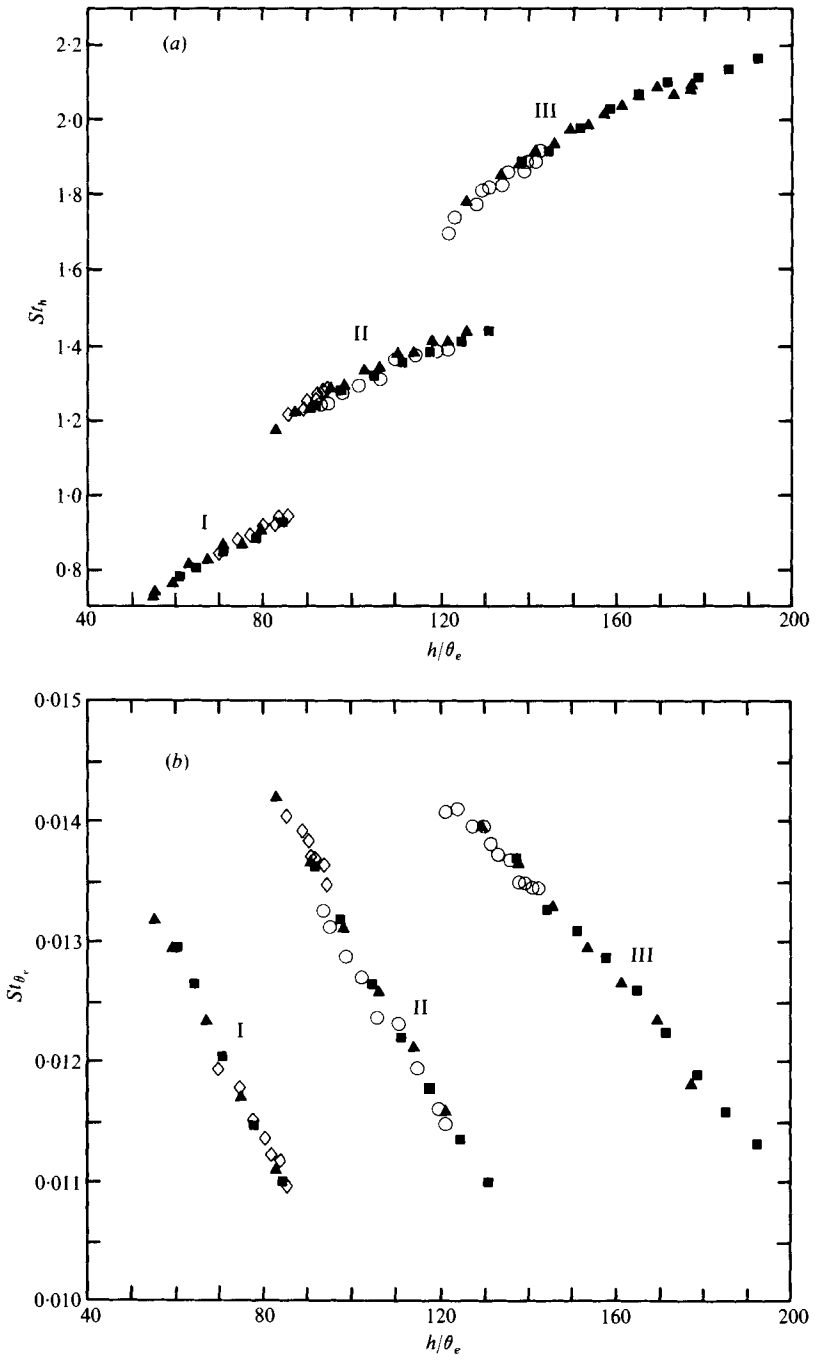

FIGURE 15. (*a*) Strouhal number St_h of the plane free shear layer tone as a function of h/θ_e for different stages. (*b*) Strouhal number $St_{\theta_e}(=f\theta_e/U_e)$ as a function of h/θ_e for different stages. The four data symbols represent the same four cases as in figure 14.

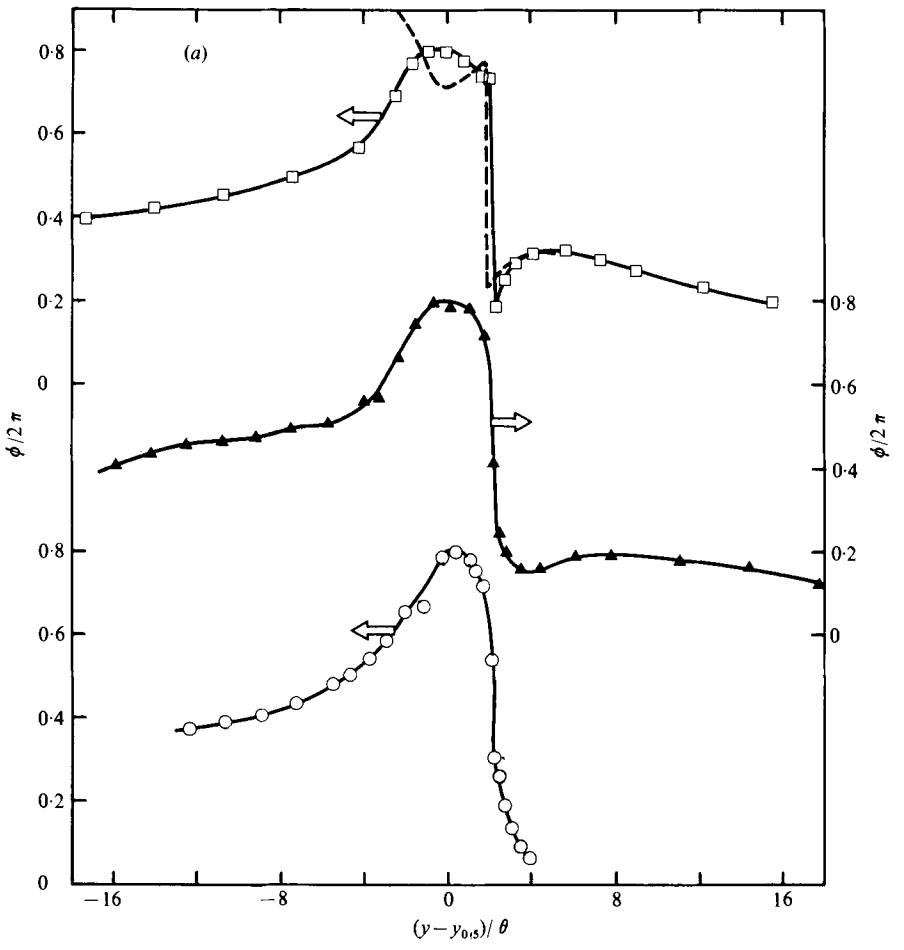

FIGURE 16(*a*). For legend see opposite.

Figures 15(*a*, *b*) clearly point out the importance of initial shear layer thickness as a scaling parameter in the shear tone. The congruence of non-dimensional frequency data in each stage for four independent cases suggests that for each stage both $St_{\theta e}$ and St_h are universal functions of the ratio of the two length scales of the problem, viz. h and θ_e. Thus either figure 15(*a*) or 15(*b*) predicts the shear layer tone frequency for any combination of h and U_e for a particular free shear layer. That is, provided the variation of θ_e as a function of U_e is known for a free shear layer in a given configuration, one should be able to predict from figure 15(*a*) or 15(*b*) the free shear layer tone frequency at any h for each U_e or at any U_e for each h. Figures 15(*a*, *b*) are thus key figures capturing the physics of the free shear layer tone phenomenon. These figures suggest that the shear layer tone is a function of the initial condition (Hussain 1977).

3.3. *Shear layer tone eigenvalues and eigenfunctions*

The free shear layer tone study would be incomplete without an understanding of the tone induced velocity amplitude variations across the layer, as well as the dependence of the wavenumber and phase velocity on the tone frequency. These data would

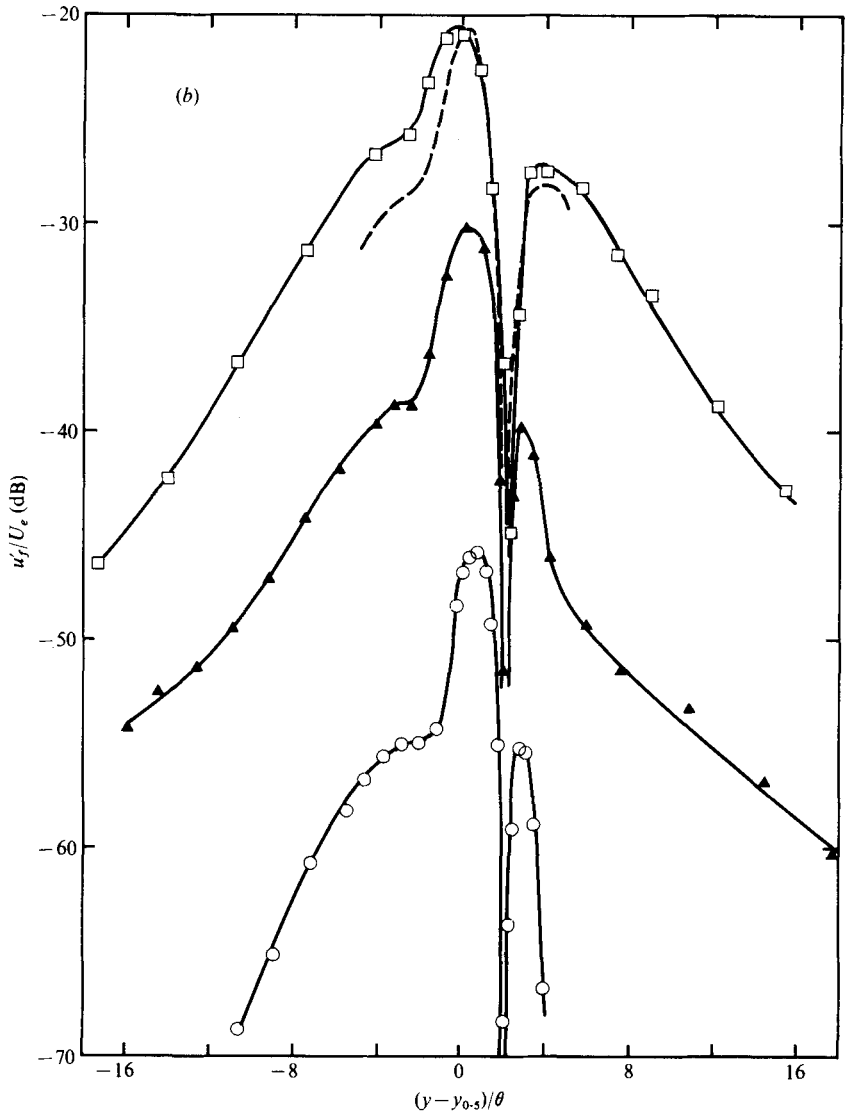

FIGURE 16. (*a*) Transverse phase variation of the shear layer tone fundamental for the plane free shear layer at $U_e = 37{\cdot}2$ m/s. Wedge at $h = 1{\cdot}4$ cm producing tone at $f = 3500$ Hz (stage II). ○, $x = 0{\cdot}508$ cm; ▲, $x = 0{\cdot}762$ cm; □, $x = 1{\cdot}016$ cm; – – –, spatial stability theory, for $x = 1{\cdot}016$ cm (Michalke 1965). (*b*) Transverse (r.m.s.) amplitude variations of the shear layer tone fundamental corresponding to three axial stations. The data symbols represent the same cases as in figure 16 (*a*). – – –, spatial stability theory, for $x = 1{\cdot}016$ cm (Michalke 1965).

represent the eigenfunctions and the eigenvalues of the shear layer tone flow; a successful shear layer tone theory must be able to predict these eigenfunctions and eigenvalues given the flow parameters, viz. h, U_e, θ_e, etc. These measurements were made in the plane free shear layer at the values of U_e: 29·3 m/s, 37·2 m/s and 43·3 m/s with the plane wedge. For a fixed wedge location at a constant U_e, a reference hot-wire probe was placed at a fixed location in the flow (figure 1 *a*). The tone frequency was determined from the spectrum of the reference probe signal. The lock-in-amplifier

was then tuned (calibrated) at this frequency. The signal from the reference probe was (narrow) band-pass filtered before it was used as the reference signal in the lock-in-amplifier. The second probe was traversed in x and y and its signal was analysed by the lock-in-amplifier to determine the relative phase of the fundamental component of the shear tone induced velocity with respect to the reference signal.

3.3.1. *Shear layer tone amplitude and phase profiles.* The transverse variation of the phase of the tone induced velocity fluctuation across the plane shear layer is shown in figure 16(*a*), for three axial locations of the signal probe. This figure corresponds to the wedge fixed at $h = 1{\cdot}40$ cm while the tone frequency was 3500 Hz; note that the phase jump occurs on the low-speed side of the half-mean velocity point, i.e. $(y - y_{0{\cdot}5})/\theta = 0$. All three figures have the same abscissa and ordinate, but the figures are shifted vertically by arbitrary amounts in order to avoid overlaps.

The dotted curve represents the theoretical phase prediction according to the spatial stability theory (Michalke 1965; Freymuth 1966) corresponding to the station $x = 1{\cdot}02$ cm. Even though the details of the theoretical profile do not agree well with the data, the agreement on the location and extent of phase jump is impressive. Other reasons for disagreement between the data and the stability theory were discussed in connexion with the probe-induced tone data in figure 3.

Figure 16(*b*) shows the profiles of the r.m.s. amplitude of the tone-induced velocity fundamental u_f' corresponding to the three phase profiles shown in figure 16(*a*). Note that the tone velocity amplitudes increase in x. The data in figure 16(*b*) were obtained to check the speculation made while discussing the data of figure 3 that, compared with the probe-induced tone case, the plane-wedge-induced tone velocity amplitude profile will agree more closely with the spatial stability theory prediction. In spite of the various reasons for expecting discrepancy between the theory and the data (discussed in § 3.1.1), the agreement on the location of the notch in figure 16(*b*) and on the location and extent of the phase jump in figure 16(*a*) for the $x = 1{\cdot}02$ cm case is very good.

3.3.2. *Phase velocity and wavenumber.* From the phase profiles in figure 16(*a*), difficulties encountered in phase velocity measurements should be obvious. Owing to large transverse phase gradients, the uncertainty in phase velocity measurements, unless done judiciously, can be excessive. For example, the phase velocity, when calculated from phase data on a y = constant line, would vary from that determined along a U/U_e = constant line.

The following criterion was adopted for finding the propagation characteristics of the shear-tone-induced velocity disturbances. For a fixed location of the wedge, the signal hot-wire probe was traversed in y at each x station to find the maximum phase ϕ_m at that x. The rate of change of this maximum phase with axial distance, $d\phi/dx$, was then found over a short axial distance Δx covering at least six closely placed data stations. The variations $\phi(x)$ were observed to be linear within the axial distance $0{\cdot}50\text{ cm} < x < 0{\cdot}9\text{ cm}$, with the reference probe held fixed at $x = 0{\cdot}914$ cm. A mean straight line though the phase data within this x range gave $d\phi/dx$, from which the phase velocity was determined.

The shear-layer-tone-induced velocity wave characteristics can be determined from the assumption of a spatially travelling vorticity wave (Lin 1955; Hussain 1970; Hussain & Reynolds 1972) in a free shear layer which acts as the waveguide. While instability of the shear layer appears to be a central factor in the shear tone pheno-

f (hz)	Stage of operation	Lip–wedge distance h (cm)	$\alpha_r = \frac{\Delta\phi}{\Delta x}\left(\frac{\text{deg}}{\text{cm}}\right)$	$\frac{v_c}{U_e}$	$\frac{h}{\lambda}$	$\frac{2\pi\theta_e}{\lambda}$
3100	I	1·138	−492	0·610	1·56	0·116
	II	1·750	−494	0·607	2·40	0·117
3300	I	1·041	−544	0·598	1·57	0·128
	II	1·598	−546	0·586	2·42	0·129
3500	I	0·914	−637	0·531	1·62	0·150
	II	1·440	−640	0·531	2·55	0·150
3700	I	0·813	−719	0·498	1·62	0·169
	II	1·334	−711	0·503	2·64	0·167

TABLE 1. Phase variation data for stages I and II at $U_e = 37{\cdot}2$ m/s.

menon, figures 16(*a*, *b*) show that the measured wave characteristics do not truly represent a (single) normal mode. However, for the purpose of determination of the wave characteristics of the shear layer tone, the non-parallel aspect will be ignored and the measured quantities will be assumed to represent a spatially dependent normal mode. Thus we can represent the instantaneous longitudinal velocity fluctuation u due to a shear tone mode as

$$u(x,y,t) = \tfrac{1}{2}\{\hat{u}(y)\exp[i(\alpha x - \omega t)] + \text{complex conjugate}\}, \tag{3}$$

where $\hat{u}(y)$ is the complex amplitude distribution in the transverse (y) direction, $\alpha = \alpha_r + i\alpha_i$ the complex wavenumber and $\omega/\alpha = c$ is also complex, i.e. $c = c_r + ic_i$, the measured phase velocity or celerity being given by $v_c = \omega/\alpha_r$. Note that figure 16(*b*) shows the amplitude profiles $|\hat{u}(y)|$ at three stations in the shear layer tone flow. When normalized by the peak values, the three amplitude profiles would indicate a certain extent of streamwise homogeneity, thus essentially justifying the parallel flow assumption.

Within the approximation stated above, it is now possible to estimate the propagating wave characteristics (α_r or λ, α_i, v_c) from the hot-wire data. From (3), it follows that at two streamwise locations x_1 and x_2, both at the same y location,

$$\frac{u(x_2,y,t)}{u(x_1,y,t)} = \exp[-\alpha_i(x_2-x_1) + i\alpha_r(x_2-x_1)]. \tag{4}$$

Denoting the phase of u by ϕ_u, i.e.

$$\phi_u(x_2,y,t) = \phi_u(x_1,y,t) + \alpha_r(x_2-x_1), \tag{5}$$

we can find λ as

$$\lambda = \frac{2\pi}{\alpha_r} = \frac{2\pi(x_2-x_1)}{\phi_u(x_2)-\phi_u(x_1)}. \tag{6}$$

The same tone frequency can be obtained in either stage I or stage II by properly locating the wedge in the axial direction. For four such frequencies, at $U_e = 37{\cdot}2$ m/s, it was found that the phase velocity was dependent on the frequency alone and not on the stage of the tone. Data (table 1) show negligible dependence of the phase velocity as well as the wavenumber on the stage of the shear tone. As already discussed, the y location of the signal probe was slightly adjusted at each x

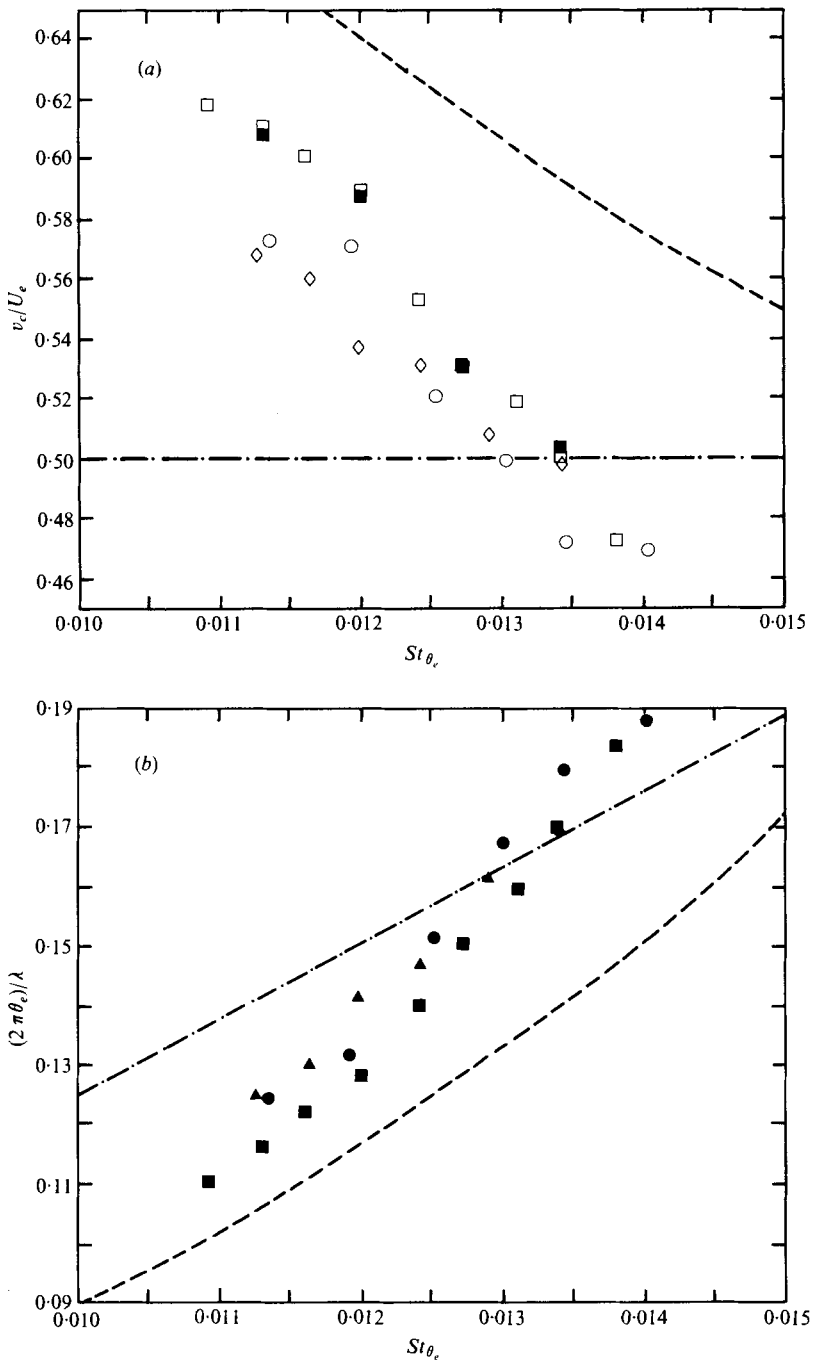

FIGURE 17. (*a*) Variation of the phase velocity v_c with the plane shear layer tone non-dimensional frequency St_{θ_e}. All the data except the four represented by the solid squares were obtained with stage I operation. ◇, $U_e = 29{\cdot}3$ m/s; □, $U_e = 37{\cdot}2$ m/s; ■, $U_e = 37{\cdot}2$ m/s (stage II operation); ○, $U_e = 43{\cdot}3$ m/s. – – –, spatial theory (Michalke 1965); —·—, temporal theory (Michalke 1965). (*b*) Variation of the non-dimensional wavenumber of the plane free shear layer tone as a function of St_{θ_e} for stage I. ▲, $U_e = 29{\cdot}3$ m/s; ■, $U_e = 37{\cdot}2$ m/s; ●, $U_e = 43{\cdot}3$ m/s; – – –, spatial theory (Michalke 1965); —·—, temporal theory (Michalke 1965).

station in order to locate the maximum phase; these y adjustments being extremely small, the line connecting the maximum phase locations may be regarded as essentially at constant y. Note that the phase profiles in figure 16 (a) cover an x range larger than that used in the determination of v_c and λ.

The phase velocity v_c was then found for different frequencies spanning the range available for the first stage of operation as indicated in figure 4. The v_c data, including those at two other speeds, are plotted as a function of the frequency (i.e. Strouhal number) in figure 17 (a). Note that for the first two stages of the $U_e = 37{\cdot}2$ m/s case the v_c data are independent of the stage and depend only on f. In the different works on shear layer instabilities and organized structures (e.g. Browand & Laufer 1975; Hussain & Thompson 1975) comparable values of the phase velocity have been reported. Note that disturbance propagation velocity decreases with increasing frequency.

The shear layer tone wavenumber as a function of $St_{\theta e}$ is plotted in figure 17 (b) for the first stage of the same three cases used in figure 17 (a). The wavelength increases with decreasing frequency in each stage. The theoretical predictions based on the spatial and temporal instability theories of Michalke (1965) for the same St_θ range are also shown for comparison. As stated earlier (§ 3.1.1), there are various differences between the theory and the real flow; any of those could explain the lack of agreement between the wavenumber and phase velocity data and the theory (figures 17 a, b). However, the trend of the data appears to agree qualitatively with the spatial instability theory. Note that Freymuth's (1966) data in a free shear layer under excitation agreed with the spatial theory at lower Strouhal number St_θ but with the temporal theory at higher St_θ. On the other hand, Crow & Champagne (1971) found close agreement of their experimental eigenvalue data with the temporal theory. While the spatial theory is expected to be the appropriate one for our experiment, it may still be inadequate to predict the data. When the non-parallel nature of the mean flow is taken into account in the spatial theory, variations of v_c/U_e and $2\pi\theta_e/\lambda$ with $St_{\theta e}$ would agree with the data more closely than shown in figure 17(a, b) (P. J. Morris, private communication). Note that θ is essentially equal to θ_e within the x range over which v_c and λ have been measured (figure 10), thus justifying use of $St_{\theta e}$ in figure 17 (a, b).

Since the phase velocity and wavelength are found to be unique functions of the free shear layer tone frequency in each stage, a cross-plot of v_c/U_e as a function of h (or U_e) would show a jump in v_c and λ at the location of a frequency jump. That is, as h is increased at a fixed U_e, both λ and v_c will increase monotonically in one stage, then drop at the start of the next stage. This result is in contrast with the data presented by Sarohia (1977), who found a smooth variation of the phase velocity during a frequency jump. For a particular stage of operation, however, the increase in phase velocity with decreasing shear tone frequency in our data is in qualitative agreement with Sarohia's data.

For a constant h, we have found that v_c/U_e increases with increasing U_e, thus suggesting that the feedback is not instantaneous or hydrodynamic. If it were so, v_c/U_e would be constant. On the other hand, increasing delay due to feedback with increasing U_e would require v_c/U_e to increase also. This is what the data show. This aspect is also being investigated currently.

3.3.3. *The h–λ relation.* The values of h/λ as a function of $St_{\theta e}$ for $U_e = 29{\cdot}3$, $37{\cdot}2$

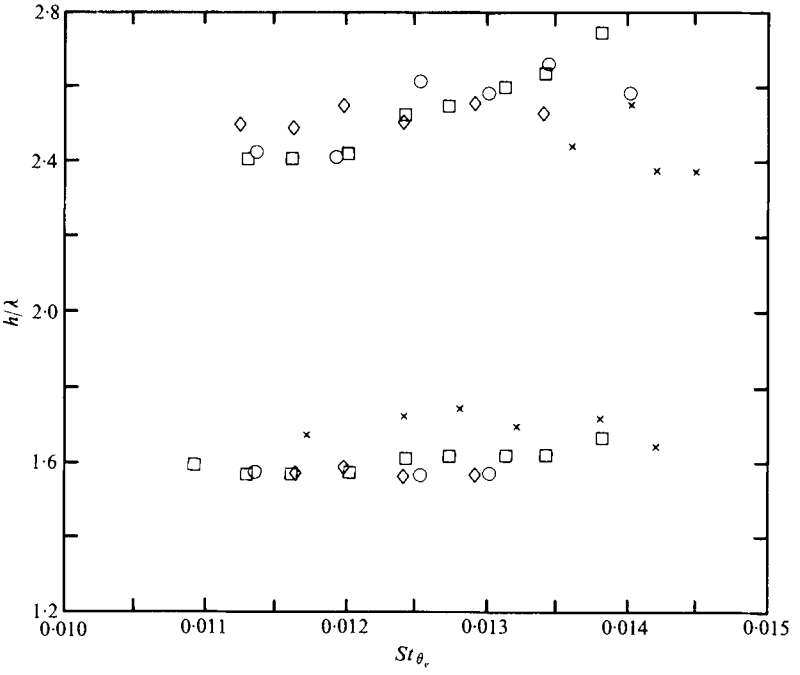

FIGURE 18. Variation of the ratio h/λ with the shear layer tone frequency St_{θ_e} for stages I and II. ◇, $U_e = 29{\cdot}3$ m/s; □, $U_e = 37{\cdot}2$ m/s; ○, $U_e = 43{\cdot}3$ m/s; ×, Sarohia (1977).

and 43·3 m/s are shown in figure 18 for the first two stages. In the slit-jet edge tone, Brown (1937*a*) showed that the ratio h/λ is not a whole number, even though it is approximately a constant in each stage of operation. Curle (1953) hypothesized from different available data on edge tone, including Brown's, that the ratio bears a relationship of the form of (2). The present data in figure 18 show that the ratio is essentially a constant in each stage; however, there is a slight increase with increasing frequency, the rate of increase being higher for stage II. The mean value of the quantity h/λ in stage I is about 1·6 while that in stage II is about 2·5; thus the constant in the free shear layer tone is different from 0·25 in the Brown–Curle equation (2) for jet edge tone. This difference should remind one that the instability mechanism in the free shear layer tone differs from that in a jet edge tone phenomenon. Note that Sarohia's (1976) data are in good agreement with ours (figure 18).

4. Concluding remarks

The hot-wire probe has been found to induce stable upstream oscillations in a free shear layer, similar to the jet edge tone mechanism. It is surprising that no previous investigator has reported this effect. This effect can be significant also in measurements involving large-scale organized structure, conditional sampling, space–time correlation, convection velocity, etc., when a reference or indicator probe may be used near the origin of the free shear layer. Such a probe can alter the instability frequency, the roll-up, the subsequent vortex coalescences, and thus the downstream large-scale coherent structure as well as the shear layer integral measures.

It appears that even in a free shear layer without any wedge, an object in the flow sufficiently downstream can also provide feedback to the flow upstream. In fact, the influence of the detection hot wire on the vortex shedding behind a cylinder, observed by Kovasznay (1949) and others, may be due to the effect studied here. On the other hand, in a turbulent free shear layer the coherent structure at a location can be the result of organization by feedback from the large-scale coherent structures further downstream (Dimotakis & Brown 1976; Naudascher 1967). The shear tone mechanism may also make a turbulent free shear layer sensitive to downstream boundary conditions.

The present study should caution against unsuspecting use of invasive probes in the near field of a free shear layer as shear tones are likely to be formed for $h \lesssim 200\theta_e$ and $d \lesssim 5\theta_e$. The unstable frequency measured by a hot wire can be altered by about 20 % owing to the shear layer tone which, however, can be taken advantage of in measuring the most unstable frequency of the free shear layer. When h is varied gradually, the tone frequency at which the velocity oscillation is the largest identifies the most unstable frequency.

The characteristics of the probe- or wedge-induced tone in a single free shear layer are found to be somewhat similar to those of the slit jet–wedge edge tone phenomenon. In any stage of operation, the tone frequency is directly proportional to the shear layer characteristic velocity scale U_e and nearly inversely proportional to the lip–wedge distance h. Detailed data pointed out some differences from published jet edge tone data; these differences are summarized below.

The free shear layer tone phenomenon does not appear to involve hysteresis in the frequency jumps between stages, as is observed in jet edge tone. During a transition, the phenomenon was found to occur only in one mode at a time while randomly flipping between the two modes, and thus contrasts the jet edge tone where simultaneous existence of two modes (stages) has been reported. In any stage of operation, the non-dimensional frequency St_h is not found to remain constant as is the case in jet edge tone; St_h increases linearly with h. The shear tone data have been shown tc fall on the same smooth curves in each stage on a St_h (or $St_{\theta e}$) *vs.* h/θ_e plot, thus permitting prediction of shear layer tone frequency for each choice of h, U_e flow configuration (geometry), and initial condition (e.g. θ_e). These data confirm that θ_e, along with h, is an important length scale of the shear layer tone phenomenon. Present data show evidence of existence of $h_{\min}$ for shear tone to occur at each U_e. However, there is no clear evidence of a corresponding $h_{\max}$ beyond which the tone will not occur.

The occurrence of the subharmonic frequency in this study is attributed to vortex coalescence. It appears that in the presence of periodic feedback, the coalescence, which otherwise occurs randomly in space and time, is organized and somewhat accentuated, thus giving an identifiable subharmonic spectral peak.

The amplitude and phase profiles of the shear layer tone induced velocity fundamental, as well as dependence of phase velocity and wavenumber on the Strouhal number show good agreement with the linear spatial instability theory of Michalke (1965); agreement with the data will be improved when the non-parallel effect is included in the spatial theory. The h–λ relation is found to be different from the Brown–Curle equation for jet edge tone. For the first two stages, the relation is found to be $h \simeq (J + C_1)\lambda$; the parameter C_1 varies somewhat from stage to stage and is about 0·5.

From our data it is apparent that instability of the free shear layer, and the lip–wedge distance h must be the key factors to produce its tone. The initial velocity profile and thus its characteristic length scale like initial momentum or vorticity thickness will affect its instability. The instability of the free shear layer is the pre-condition for shear tone; the wedge has no influence on the shear layer instability, other than to provide positive feedback to the sensitive point, i.e. the lip, and organize the otherwise randomly occurring instability, nonlinear saturation and vortex roll-up. A particular mode finds stable amplification through the tone feedback when the corresponding most unstable wavelength matches appropriately with the lip–wedge distance, or stated another way, when the shear layer instability induced disturbance at the wedge arrives at the lip at the correct phase to provide positive feedback and sustain the instability.

It appears that the non-parallel aspect of the shear layer instability is not the central factor in shear tone behaviour. Further details of the shear layer tone and the role of instability are currently being investigated in our laboratory.

We are grateful to the National Science Foundation and the NASA Langley Research Center for financial support; to Professor G. H. Koopmann for a careful review of the manuscript; and to him and Professors Anatol Roshko, Hans Liepmann, John Laufer and I. Wygnanski for stimulating discussions on our data.

REFERENCES

Bilanin, A. J. & Covert, E. E. 1973 *A.I.A.A. J.* **11**, 347.

Bishop, K. A., Ffowcs Williams, J. E. & Smith, W. 1971 *J. Fluid Mech.* **50**, 21.

Bolton, S. 1976 M.Sc. thesis, University of Southampton.

Bradshaw, P. 1966 *J. Fluid Mech.* **26**, 225.

Browand, F. K. & Laufer, J. 1975 *Turb. Liquids, Univ. of Missouri-Rolla*, **5**, 333.

Browand, F. K. & Weidman, P. D. 1976 *J. Fluid Mech.* **76**, 127.

Brown, G. & Roshko, A. 1974 *J. Fluid Mech.* **64**, 775.

Brown, G. B. 1937*a* *Proc. Phys. Soc.* **49**, 493.

Brown, G. B. 1937*b* *Proc. Phys. Soc.* **49**, 508.

Corcos, G. M. & Sherman, F. S. 1976 *J. Fluid Mech.* **73**, 241.

Crow, S. C. & Champagne, F. H. 1971 *J. Fluid Mech.* **48**, 547.

Curle, N. 1953 *Proc. Roy. Soc.* A **216**, 412.

Dimotakis, P. E. & Brown, G. L. 1976 *J. Fluid Mech.* **78**, 535.

Freymuth, P. 1966 *J. Fluid Mech.* **25**, 683.

Hussain, A. K. M. F. 1970 Ph.D dissertation, Stanford University.

Hussain, A. K. M. F. 1977 Initial condition effect on free turbulent shear flows. *Symp. Turbulence, Berlin.*

Hussain, A. K. M. F. & Clark, A. R. 1977 *Phys. Fluids* **20**, 1416.

Hussain, A. K. M. F. & Reynolds, W. C. 1972 *J. Fluid Mech.* **54**, 241.

Hussain, A. K. M. F. & Thompson, C. A. 1975 *Proc. 12th Ann. Meeting, Soc. Engng Sci., Univ. Texas (Austin)*, pp. 741–752.

Hussain, A. K. M. F. & Zaman, K. B. M. Q. 1975 *Proc. 3rd Int. Symp. Trans. Noise, Univ. of Utah*, pp. 314–326.

Hussain, A. K. M. F. & Zaman, K. B. M. Q. 1977 Controlled perturbations of circular jets. *Symp. Turbulence, Berlin.*

HUSSAIN, A. K. M. F. & ZEDAN, M. F. 1977 Effects of the initial condition on the axisymmetric free shear layer: effect of the initial fluctuation level. *Phys. Fluids* **21** (in press).

KARAMCHETI, K., BAUER, A. E., SHIELDS, W. L., STEGEN, G. R. & WOOLLEY, J. P. 1969 *N.A.S.A. Special Paper* no. 207, p. 275.

KLINE, S. J., COLES, D. E., EGGERS, J. M. & HARSHA, P. T. 1973 *N.A.S.A. Special Paper* no. 321, p. 655.

KO, N. W. M. & DAVIES, P. O. A. L. 1971 *J. Fluid Mech.* **50**, 49.

KO, N. W. M. & KWAN, A. S. H. 1976 *J. Fluid Mech.* **73**, 305.

KOVASZNAY, L. S. G. 1949 *Proc. Roy. Soc.* A **198**, 174.

KOVASZNAY, L. S. G. 1977 Large scale structures in turbulence – a question or an answer? *Symp. Turbulence, Berlin.*

LAMB, H. 1945 *Hydrodynamics.* Dover.

LIEPMANN, H. & LAUFER, J. 1947 *N.A.C.A. Tech. Note* no. 1257.

LIN, C. C. 1955 *The Hydrodynamic Stability Theory.* Cambridge University Press.

LING, C. & REYNOLDS, W. C. 1973 *J. Fluid Mech.* **59**, 571.

LIU, J. T. C. 1974 *J. Fluid Mech.* **62**, 437.

MCCANLESS, G. F. & BOONE, J. R. 1974 *J. Acoust. Soc. Am.* **56**, 1501.

MICHALKE, A. 1965 *J. Fluid Mech.* **23**, 521.

MICHALKE, A. 1972 *Prog. Aero. Sci.* **12**, 213.

MOORE, D. W. & SAFFMAN, P. G. 1975 *J. Fluid Mech.* **69**, 465.

NAUDASCHER, E. 1967 *Proc. A.S.C.E.* **93**(HY4), 15.

NYBORG, W. L. 1954 *J. Acoust. Soc. Am.* **26**, 2.

POWELL, A. 1961 *J. Acoust. Soc. Am.* **33**, 4.

RICHARDSON, E. G. 1931 *Proc. Phys. Soc.* **43**, 394.

ROSHKO, A. 1976 *A.I.A.A. J.* **10**, 1349.

SAROHIA, V. 1977 *A.I.A.A. J.* **15**, 984.

SATO, H. 1960 *J. Fluid Mech.* **7**, 53.

WINANT, C. D. & BROWAND, F. K. 1974 *J. Fluid Mech.* **63**, 237.

WOOLLEY, J. P. & KARAMCHETI, J. 1974 *A.I.A.A. J.* **12**, 1457.

ZAMAN, K. B. M. Q. & HUSSAIN, A. K. M. F. 1977 *Proc. Symp. Turbulent Shear Flow, Penn. State Univ.*, pp. 11.23–11.31.